

2011

Molecular Dynamic Simulation of Thin Film Growth Stress Evolution

Haifeng Zheng
Lehigh University

Follow this and additional works at: <http://preserve.lehigh.edu/etd>

Recommended Citation

Zheng, Haifeng, "Molecular Dynamic Simulation of Thin Film Growth Stress Evolution" (2011). *Theses and Dissertations*. Paper 1256.

This Thesis is brought to you for free and open access by Lehigh Preserve. It has been accepted for inclusion in Theses and Dissertations by an authorized administrator of Lehigh Preserve. For more information, please contact preserve@lehigh.edu.

**Molecular Dynamic Simulation of Thin Film Growth
Stress Evolution**

by

Haifeng Zheng

A Thesis

Presented to the Graduate and Research Committee

of Lehigh University

in Candidacy for the Degree of

Master of Science

in

Mechanical Engineering and Mechanics Department

Lehigh University

September, 2011

This thesis is accepted and approved in partial fulfillment of the requirements for the Master of Science.

Date

Thesis Advisor

Prof. Edmund B. Webb

Chairperson of Department

Prof. D. Gary Harlow

ACKNOWLEDGEMENTS

I would like to express my gratitude to my advisor, Prof. Edmund B. Webb, for providing me with his valuable advice, friendship and many insightful conversations through the research process. I also extend thanks to Steve Lidie and Ovidiu Dan for teaching and helping me about high performance computing at Lehigh University. Thank to professors in MEM department and my colleagues for helpful comments and support on this work. Finally, I would like to express my gratitude to my family who always support and encourage me no matter what decision I made.

Table of Contents

List of Tables	v
List of Figures	vi
Abstract	1
Chapter 1 Introduction	3
Chapter 2 Background Information	10
2.1 Thin Film Growth Methods	11
2.1.1 Physical Vapor Deposition	14
2.1.2 Chemical Deposition.....	20
2.1.3 Comparison of Typical Thin Film Deposition Technology.....	23
2.2 Thin Films Growth Modes	24
2.3 Stresses Evolution in Thin Films	28
2.3.1 Compressive Stress in the Discrete-Island Regime	31
2.3.2 Tensile Stress in the Island-Coalescence Regime.....	33
2.3.3 Postcontinuity Compressive Stress	37
2.4 Stresses Measurement and Analysis Technology	39
Chapter 3 Numerical Procedure	42
3.1 Numerical Simulations.....	42
3.2 Molecular Dynamics Simulations	44
3.2.1 Molecular Interaction.....	46
3.2.2 Integrator.....	47
3.2.3 Ensembles	48
3.3 Simulations Description	50
3.4 Simulation Procedures.....	53
Chapter 4 Results and Discussions	60
4.1 Initial Coalescence Stress Analysis.....	60
4.2 Intrinsic Stress Evolution Behavior	73
Chapter 5 Summary and Future Work	98
Reference	100
VITA	103

LIST OF TABLES

Table 1 Thin film categories and applications	4
Table 2 Comparison of Typical Thin Film Deposition Technologies	24
Table 3 Geometry of computational domain	56
Table 4 Initial coalescence stress	62

LIST OF FIGURES

Figure 1-1 Multilayer thin-film sensor	5
Figure 1-2 Schematic of structure of thin film transistors	6
Figure 1-3 Face centered cubic structure: orange larger balls and purple smaller balls stand for lattice points on the corners and on the faces, respectively.	8
Figure 2-1 Thin film process steps.....	13
Figure 2-2 Schematic of thermal evaporation deposition	15
Figure 2-3 Schematic of “planetary configuration”	16
Figure 2-4 Ion beam sputtering system.....	19
Figure 2-5 Typical hot-wall LPCVD reactor	21
Figure 2-6 Typical setup for electrodeposition	23
Figure 2-7 Cross-section views of the three Primary modes of thin film growth including (a) Volmer-Weber, (b) Frank-Van der Merwe, and (c) Stranski-Krastanov. Each mode is shown for several different amounts of surface coverage θ	25
Figure 2-8 Film forces per unit width against mean thickness (left-hand side) and time (right-hand size) of Ag films UHV deposited onto mica(001) at various substrate temperatures. By convention positive and negative values denote tensile and compressive forces, respectively.	30
Figure 2-9 Views of (a) coalescence geometry used in Hoffman’s analysis, (b) coalescence geometry used in Nix and Clemens’s analysis, and (c) coalescence geometry used in Freund and Chason’s analysis. Dashed lines in (a) and (b) represent the shape of islands just prior to coalescence.....	35
Figure 2-10 Schematic of model for flow of atoms into, and out of the grain boundaries by change in surface potential.....	38
Figure 3-1 Schematic comparison of time- and length-scales, accessible to different types of simulation techniques (quantum mechanics (DFT), classical atomistic (MD, MC), mesoscale methods and continuum (FE, FD)).....	43
Figure 3-2 Structure of “Island-Substrate” system before deposition, including three zones: (a) frozen zone, (b) substrate, and (c) islands	51
Figure 3-3 Structure of “Island-Substrate” system after deposition, including a grain boundary and three zones: (a) frozen zone, (b) substrate, and (c) islands	51

Figure 3-4 Schematic of computational domain.....	55
Figure 3-5 Schematic of computational domain II. Dashed line configurations indicate infinite array of uniform islands in x direction.	57
Figure 3-6 Schematic of computational domain III.....	58
Figure 4-1(a) Histogram of stress for 5 nm substrate system at 0 picosecond	64
Figure 4-1(b) Histogram of stress for 5 nm substrate system at 1 picosecond	64
Figure 4-1(c) Histogram of stress for 5 nm substrate system at 10 picoseconds.....	65
Figure 4-1(d) Histogram of stress for 5 nm substrate system at 500 picoseconds	65
Figure 4-2(a) Histogram of stress for 10 nm substrate system at 0 picosecond	66
Figure 4-2(b) Histogram of stress for 10 nm substrate system at 10 picoseconds	66
Figure 4-2(c) Histogram of stress for 10 nm substrate system at 500 picoseconds.....	67
Figure 4-3(a) Histogram of stress for 20 nm substrate system at 0 picosecond	67
Figure 4-3(b) Histogram of stress for 20 nm substrate system at 10 picoseconds	68
Figure 4-3(c) Histogram of stress for 20 nm substrate system at 500 picoseconds.....	68
Figure 4-4(a) Stress distribution coloring for 10 nm substrate system at 0 ps of initial coalescence run. The color bar shows stress in MPa.	72
Figure 4-4(b) Stress distribution coloring for 10 nm substrate system at 500 ps of initial coalescence run	72
Figure 4-5 Intrinsic stress against effective film thickness.....	74
Figure 4-6 Force per unit width against effective film thickness	74
Figure 4-7 (a) Configuration Snapshot before the first jump (Random Seed 1)	83
Figure 4-7 (b) Configuration Snapshot after the first jump (Random Seed 1)	84
Figure 4-7 (c) Configuration Snapshot before the second jump (Random Seed 1).....	85
Figure 4-7 (d) Configuration Snapshot after the second jump (Random Seed 1)	86
Figure 4-8 (a) Configuration Snapshot before the first jump (Random Seed 2)	87
Figure 4-8 (b) Configuration Snapshot after the first jump (Random Seed 2)	88
Figure 4-8 (c) Configuration Snapshot before the second jump (Random Seed 2).....	89
Figure 4-8 (d) Configuration Snapshot after the second jump (Random Seed 2)	90
Figure 4-8 (e) Configuration Snapshot before the drop (Random Seed 2).....	91
Figure 4-8 (f) Configuration Snapshot after the drop (Random Seed 2)	92
Figure 4-9 (a) Configuration Snapshot at the end of simulation (Random Seed 1)	93

Figure 4-9 (b) Configuration Snapshot at the end of simulation (Random Seed 2)	94
Figure 4-9 (c) Configuration Snapshot at the end of simulation (Random Seed 3)	95
Figure 4-9 (d) Configuration Snapshot at the end of simulation (Random Seed 4)	96
Figure 4-9 (e) Configuration Snapshot at the end of simulation (Random Seed 5)	97

Abstract

With the increasing demand for thin films across a wide range of technology, especially in electronic and magnetic applications, controlling the stresses in deposited thin films has become one of the more important challenges in modern engineering. It is well known that large intrinsic stress - in the magnitude of several gigapascals - can result during the thin film preparation. The magnitude of stress depends on the deposition technique, film thickness, types and structures of materials used as films and substrates, as well as other factors. Such large intrinsic stress may lead to film cracking and peeling in case of tensile stress, and delamination and blistering in case of compression. However it may also have beneficial effects on optoelectronics and its applications. For example, intrinsic stresses can be used to change the electronic band gap of semiconducting materials. The far-reaching fields of microelectronics and optoelectronics depend critically on the properties, behavior, and reliable performance of deposited thin films. Thus, understanding and controlling the origins and behavior of such intrinsic stresses in deposited thin films is a highly active field of research.

In this study, on-going tensile stress evolution during Volmer-Weber growth mode was analyzed through numerical methods. A realistic model with semi-cylinder shape free surfaces was used and molecular dynamics simulations were conducted. Simulations were at room temperature (300 K), and 10 nanometer diameter of islands were used. A deposition rate that every 3 picoseconds deposit one atom was chosen for simulations. The deposition energy was 8.27×10^{-3} eV and lattice orientation is [0 0 1]. Five different random seeds were used to ensure average behaviors.

In the first part of this study, initial coalescence stress was first calculated by comparing two similar models, which only differed in the distance between two neighboring islands. Three different substrate thickness systems were analyzed to ensure no simulation artifacts were introduced by this parameter. Results from the calculations showed that initial coalescence stress of 5 nanometer thickness substrate system is significantly lower than that of the other two systems. Then histogram analysis and stress coloring analysis were conducted to analyze the distribution of stress within thin films. It was concluded that substrates 10 nm thick were sufficient for subsequent stress evolution simulation studies.

In the second part of this study, on-going tensile stress evolution was examined by modeling atomic scale deposition (i.e. film growth) for at least 30 nanoseconds. Intrinsic stress as a function of effective island thickness, and force per unit width as a function of effective island thickness were obtained from simulations. Average stress behaviors and corresponding atomistic structure changes were analyzed.

Chapter 1 Introduction

Thin solid films are structures whose dimensions in the plane of the film are significantly larger than the film thickness, which can span from 10^{-9} meter to 10^{-6} meter. Thin films are typically deposited on a substrate or another film. However, films can be separated from a substrate to achieve a free standing thin film. Alternatively, a single thin film may represent one layer of many in a multi-layer device such as a computer chip. These films can be viewed as two-dimensional structures since their thickness is very small relative to their lateral dimensions. However, caution must be applied with such a view since a thin film's properties can intimately depend on film thickness.

Thin films are deposited onto a substrate to achieve new properties that are unattainable in the substrates alone. The range of thin film applications is very broad indeed. Thin films can be used to modify the properties of the underlying material, e.g. to enhance the hardness, to change electrical and thermal conductivities. In other cases, thin films act as a role to support the materials above itself, or separate two layers in the devices, e.g. to isolate one conducting layer from another or to prevent interdiffusion between layers. Table 1 shows how such applications are divided into five properties and corresponding examples are given[1].

Thin film property category	Typical applications
Mechanical	Tribological (wear-resistant) coating
	Hardness
	Micromechanics
Optical	Reflective/antireflective coatings

	Interference filters
	Memory discs (CDs)
	Decoration (color, luster)
Electrical	Semiconductor devices
	Conduction
	Insulation
	Piezoelectric devices
Magnetic	Memory discs (CDs)
Chemical	Barriers to diffusion or alloying
	Protection against oxidation or corrosion
	Gas/liquid sensors

Table 1 Thin film categories and applications

Various thin films are widely used in semiconductor industry and MicroElectroMechanical System (MEMS) devices[1, 2]. MEMS is the technology of very small mechanical devices driven by electricity. Thin films are very suitable for such small and compact devices, including microactuators, sensors, micromotors and frictionless microgears. Since thin films can be produced in many forms and have properties that can differ significantly from bulk form, they play an important role in enhancing the property and performance of tools and machines. For instance, silicon dioxide (SiO_2) thin film is commonly used as an insulating layer in MEMS structures for separating a silicon substrate and device stacks on top of the substrate.



Figure 1-1 Multilayer thin-film sensor

Figure 1-1 shows a multilayer thin-film sensor used in aircraft industry. New multilayer thin films are combined with magnetostrictive sensors to nondestructively detect and monitor defects in aircraft components.

Thin films play a crucial role in the modern semiconductor industry[1, 2]. The use of thin film heterogeneous semiconductors enables the fabrication of many unique device capabilities. In semiconductor devices, thin films are used to form the conducting lines connecting individual devices, as well as the contact pads to which are bonded the wires that connect the circuit to the encapsulating structure. They are also used to isolate the conducting layer from the underlying substrate structure. An example is the widespread use of thin film transistor (TFTs), a form of field effect transistor fabricated by depositing thin films of semiconductor active layer on glass substrates. Figure 1-2 is a schematic of structure of thin film transistors. A voltage applied at the gate controls the flow of electrons from the source to the drain. Note there is an insulating layer between the semiconductor and the gate material. While this prevents direct conduction between the

two layers, the electric field in the gate interacts with the semiconductor. At sufficient voltage to the gate, charge carriers in the semiconductor concentrate and form conducting paths between the source and drain. The semiconductor active layer as well as dielectric layer (insulator) are generated by depositing thin films over a supporting substrate.

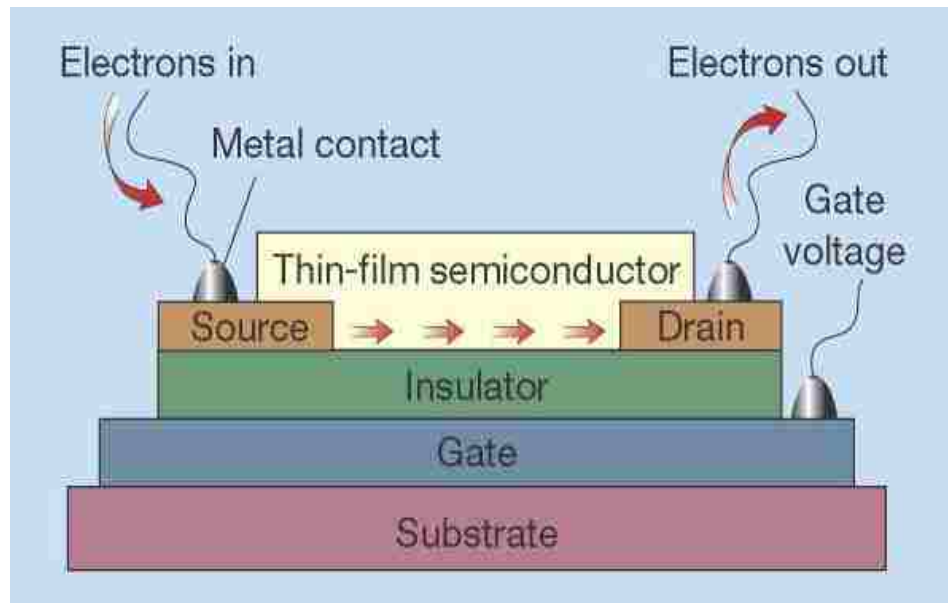


Figure 1-2 Schematic of structure of thin film transistors

Furthermore, thin film techniques are widely used in photovoltaic products. Compared to traditional solar panels, thin film photovoltaic panels use thin film technologies to reduce the cost of producing a solar panel. A thin film of CIGS (copper indium gallium selenium), which is 100 times thinner than traditional silicon semiconductors, is applied to a substrate such as glass. Such thin film photovoltaic products have a great potential in saving material and protecting our environment and, as such, they are gaining increasing attention from industry.

The economic advantage is the tremendous driving force to introduce thin films in semiconductor and electronics industries as well as thin film photovoltaic products. In a word, thin films are essential to semiconductor and MicroElectroMechanical System (MEMS) devices.

There is a wide range of materials used in different thin film applications and different thin film growth methods. Many of them can be divided into two major families: metals and semiconductor materials. The three semiconducting elements (Si, Ge, and Sn) from column IVA of the periodic table serve as a kind of boundary between metallic and nonmetallic elements. Silicon (Si) and germanium (Ge) are widely used elemental semiconductors. Within metals lots of materials used commonly are face centered cubic (FCC) metals such as Aluminum (Al), Silver (Ag), Copper (Cu), Nickel (Ni) and gold (Au). In crystallography, the cubic crystal system is a crystal system where the unit cell is in the shape of a cube. Face centered cubic (FCC) is one of three main varieties of cubic crystal system. Figure 1-3 shows Face centered cubic structure. The FCC system has six lattice points on the faces and eight lattice points on the corners of the cube. Six lattice points on the faces give exactly three atoms contribution to each unit cell, and eight lattice points on the corners give exactly one atom contribution to each unit cell. So FCC system has a total of 4 atoms per unit cell. Since a large number of FCC metals are widely used in different thin film applications, significant research has been done to understand their use in thin film applications. Such research will guide us in manufacturing processes to produce high-quality thin film products.

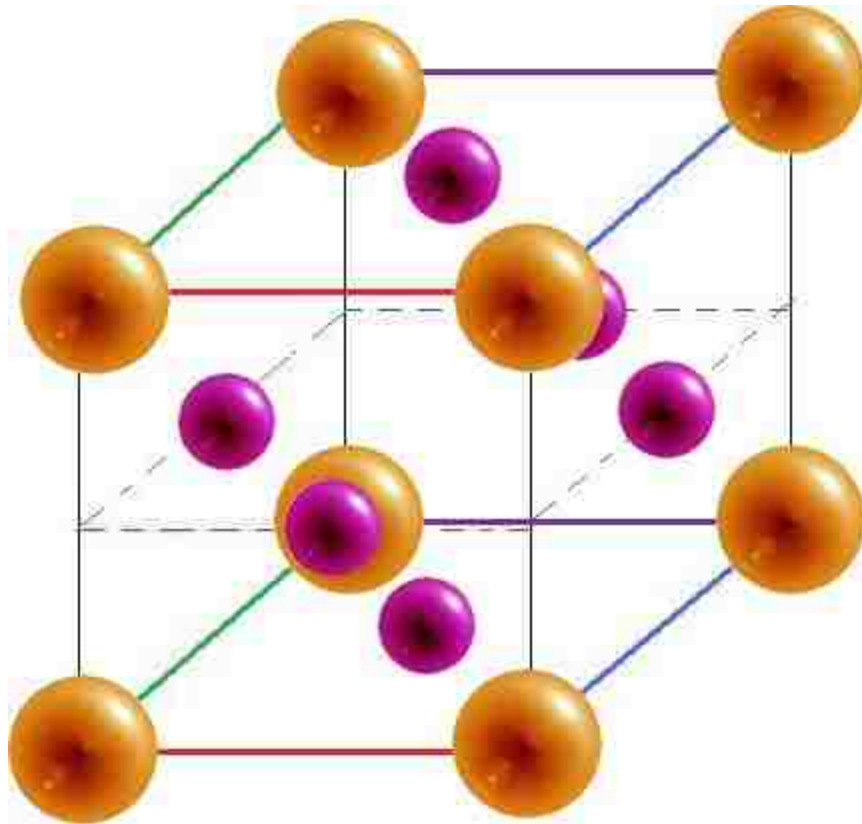


Figure 1-3 Face centered cubic structure: orange larger balls and purple smaller balls stand for lattice points on the corners and on the faces, respectively.

In the manufacturing process, the mechanical properties of thin films are of great concern since any unwanted defects can decrease and even remove a device's functionalities. The intrinsic residual stress within thin films is a big factor that leads to defects or failures in films. The magnitude of such intrinsic stresses in as-deposited thin films can be well in excess of the typical yield stresses of the corresponding materials in their bulk form. This would lead to damage and/or defects evolution in the films, which would greatly affect the quality of films. Examples of damage induced by such high level stress include film cracking, peeling, bulking and surface roughening[3, 4]. Understanding mechanisms that dictate the formation and evolution of thin film stress

and developing strategies to control these stresses represent some of the most important outstanding issues in the thin film growth community.

Furthermore, stress evolution is not typically uniform. More will be said in the following sections, but some materials exhibit significant variations in stress evolution as they grow; for example, some materials begin with compressive stress evolution, then go tensile, only to go compressive again. While some mechanisms driving such complex stress evolution are understood, many details are not. In particular, atomic scale stress evolution mechanisms are difficult to reveal via experimental methods. For this reason, atomic scale models - specifically simulations - have great power to increase our understanding of fundamental thin film stress evolution mechanisms. In this thesis, research is presented using the molecular dynamics numerical simulation method to explore atomic scale stress evolution mechanisms in thin films.

Chapter 2 Background Information

This chapter gives an overall introduction about thin films, including thin film growth methods, thin films growth modes, typically observed stress evolution within thin films, as well as intrinsic stress measurement techniques. Sections are assigned accordingly; in the first section, two broad categories of thin film deposition methods are presented: physical vapor deposition and chemical deposition. A comparison of different methods within each category is given in this section. In Thin Film Growth Modes section, a summary of three growth modes - Volmer-Weber mode, Frank-Van der Merwe mode and Stranski-Krastanov mode – are discussed, including growth behavior, morphology as well as corresponding underlying energy mechanisms that dictate which growth mode is observed. In Stress Evolution in Thin Films section, focus is placed on one commonly observed growth mode and a summary and comparison between different residual stress models during Volmer-Weber thin film growth are discussed. Global energy analysis, surface stress mechanism and excess atoms mechanism are discussed. Emphasis is placed on proposed mechanisms during tensile stress evolution during Volmer-Weber growth. At the end of chapter 2, common stress measurement and analysis techniques are introduced. Methods most commonly used can be divided into two groups: techniques that measure the bending of the substrate and diffractive methods.

2.1 Thin Film Growth Methods

In this section, general features of all styles of thin film deposition are reviewed. Following this, greater details are provided on each type of deposition. Thin film deposition is a process of adding material to a prepared substrate (e.g. a semiconductor wafer).

The methods for the deposition of thin films can be divided into two classes: physical vapor deposition and chemical deposition[1, 2]. In physical vapor deposition, a film is formed by atoms directly transported from source material through the atmosphere to the substrate. Source materials used are somehow forced to become vapor species, which are transported to a substrate. The methods to generate vapor species are various and should be chosen based on the property of source materials and thin films. The common methods include thermal evaporation, E-beam evaporation and sputtering. In chemical deposition, a film is formed by chemical reaction on the surface of a substrate. Source materials are driven to become fluids (liquid or vapor) for transportation and subsequent chemical reaction on the substrate surface. Generally chemical deposition has two families: vapor phase deposition, e.g. chemical vapor deposition (CVD), and liquid phase chemical deposition, e.g. chemical solution deposition (CSD).

Both physical deposition and chemical deposition have in common four or five procedures shown in Figure 2-1. These are the preparation of source material, source material transportation to a substrate, deposition onto the substrate, and sometimes post-deposition annealing treatment or heat treatment is used. Finally a thin film is typically

analyzed to evaluate the process. The results of analysis can be used to improve the process by adjusting processing conditions to optimize thin film properties.

To deposit a thin film, source material is first prepared. The source material can be in form of solid, liquid or vapor. In both physical and chemical vapor deposition, non-vapor source materials need to be evaporated during deposition. Then the species are transported to a substrate. The evaporation process can be done by heating (thermal) or by bombarding the source material. Bombardment is typically done with an energetic beam of electrons (E-beam), photons (laser ablation), or positive ions (sputtering). These methods are categorized as physical vapor deposition since growth of the source materials on the substrate occurs in the absence of reactions. In other cases, thin film processes that use reacting gas, liquids, or solids source materials are categorized as chemical deposition.

In the case of chemical deposition, the supply species or molecules are transported from source material to the surface of a substrate where they then undergo some chemical reactions to generate the desired deposition product. In this step, uniformity of films is an important issue; obviously, large substrates are more difficult to cover uniformly than small substrates. However different methods of transportation may have a great impact on uniformity of thin films. Compared to physical vapor deposition techniques, chemical deposition techniques tend to be conformal, which can have a better performance on uniformity. A conformal coating means that a thin film has uniform thickness in each direction; this is important, for instance, when coating non-planar surfaces. There are chemical reactions during chemical deposition, allowing atoms or

molecules to diffuse on the substrate surface. That is why that thin films from chemical deposition techniques tend to be conformal. In physical deposition, since particles tend to follow a straight path, thin films deposited by physical means are commonly directional, rather than conformal.

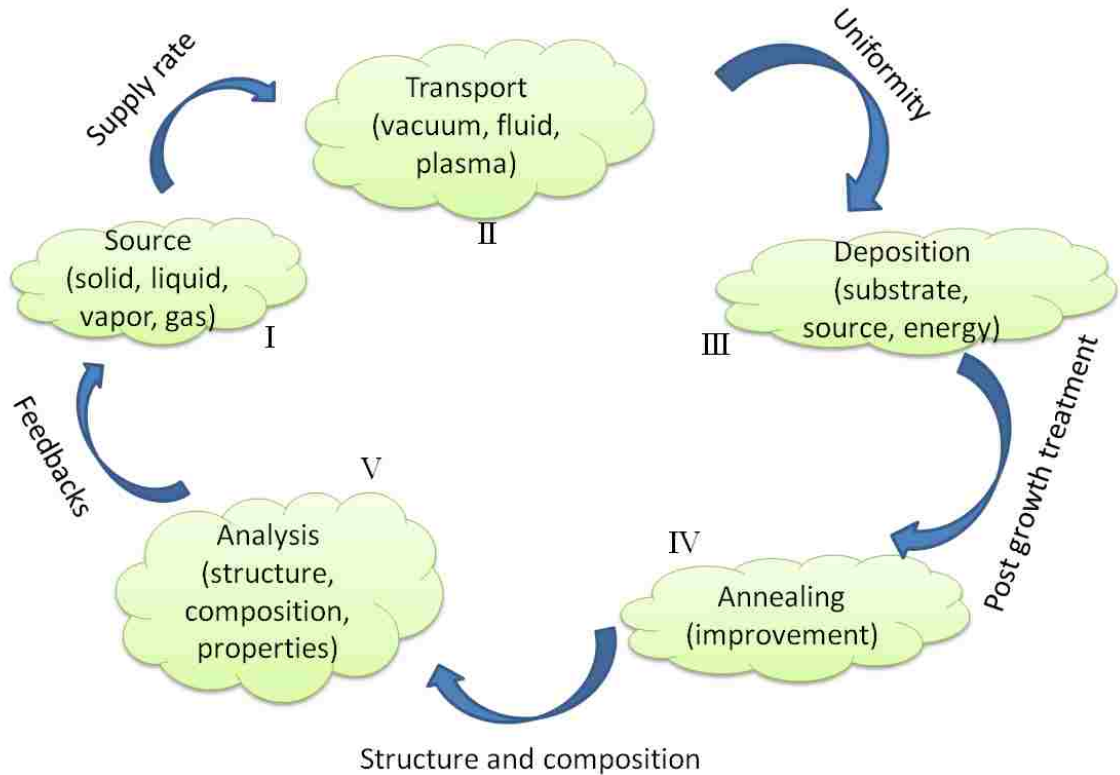


Figure 2-1 Thin film process steps

The third step is depositing supply species on the surface of the substrate. The condition of substrate surfaces is a key issue in this process. Physical vapor deposition desires an extreme clean environment in order to prevent contaminants of films, so the deposition is usually under vacuum or Ultra High Vacuum (UHV) environment. In chemical deposition techniques, reactivity of source material and energy input can also have great impact on this step.

In some cases, postgrowth treatments are taken to improve the property of thin films. For instance, for polycrystalline films comprised of many micron scale crystals or grains, annealing of the film at elevated temperature may generate a film with better properties. This occurs as a result of grain growth in the film and change in composition through mass diffusion. Grain growth refers to the increase in size of grains (crystallites) in a material at high temperature. This occurs when recovery and recrystallisation are complete and further reduction in the internal energy can only be achieved by reducing the total area of grain boundary.

The final step in deposition process is analysis of thin films. Thin film analysis employs modern analytical techniques to understand how the deposition process affects film properties. The goal is to improve the process and generate a better thin film with superior properties. Techniques such as X-ray diffraction can be used to examine the structure of thin films, or transmission electron microscopy (TEM) can be used to detect highly detailed atomistic phenomenon. Many thin film deposition techniques can be optimized by varying process variables during the first three process steps. The analysis can supply feedbacks to improve deposition results.

Though common steps exist for all deposition techniques, each deposition method has specific requirements on the deposition process. In the following section, more details are presented for each deposition method.

2.1.1 Physical Vapor Deposition

Thermal Evaporation Deposition

Thermal evaporation deposition is a physical vapor deposition method where heating (thermal energy) is used to vaporize the source material. This method has a wide applicable range. It can be used to deposit almost all metals except the highly refractory metals. Refractory metals are those with very high melting temperature, e.g. Chromium (Cr) and Tungsten (W). It is difficult to evaporate such metals due to their high melting temperature. Furthermore, it is not easy to find a suitable crucible for processing such materials.

In thermal evaporation, the film source materials are heated to the point at which sublimation or evaporation occurs, depending on the whether the source material is solid or liquid. A highly controlled environment is desired in order to get high-purity thin films. In this method, it is necessary to heat the source material to a temperature where it has significant vapor pressure.

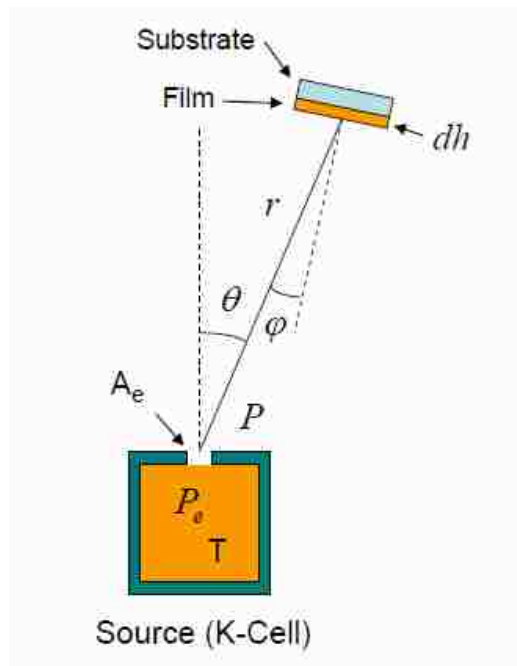


Figure 2-2 Schematic of thermal evaporation deposition

For thermal evaporation, as shown in Figure 2-2, the mass deposition rate can be calculated as

$$R_m = C_m \left(\frac{M}{T} \right)^{1/2} \cos\theta \cos\varphi \frac{1}{r^2} (P_e(T) - P) \quad (1)$$

Where R_m is mass deposition rate (per unit area of source surface), $C_m = 1.85 \times 10^{-2}$, r is source-substrate distance, T is source temperature, P_e is evaporating vapor pressure, P is chamber pressure and M is the gram-molecular mass of the evaporating material. Figure 2-3 shows the definition of φ and θ .

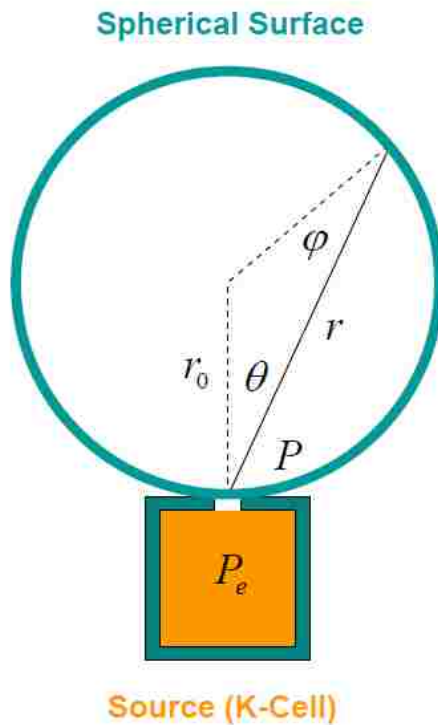


Figure 2-3 Schematic of “planetary configuration”

Uniformity is a key problem using thermal evaporation deposition in the production of integrated circuits. The source material in this case can be treated as a point

source and, in this case, the flux decreases as square of the distance between source material and substrate. Consider a point source and a large substrate: due to different distance between source and substrate as a function of position on the surface, deposition flux differs between the center and edge of substrate and thus may have great impact on uniformity. It should be noted that flux decreases as the cosine of the angle from substrate normal to the source θ . Therefore a specified arrangement of substrates and source crucible, known as “planetary configuration”, as shown in Figure 2-3, is introduced to overcome non-uniformity problems. Substrates are placed as a sphere and source crucible is set at the bottom of “substrate planetary”. In this configuration, substrate that is close to the source crucible has a big angle between the substrate normal and the source, so the distance and angle effects compensate.

E-beam Evaporation Deposition

E-beam evaporation is used for highly refractory metals with such high melting temperature that are difficult to evaporate from a resistively heated crucible. A beam of high-energy electrons from electron beam evaporators heats a small portion of source metal to a high temperature. A molten core is contained in a container of the same material. Such phenomenon is referred to as “skull molten”. “Skull molten” has the advantage in avoiding the contamination from containers. In general, refractory metals are used to contain the molten portion. High temperature may make the refractory metal evaporate into the molten portion resulting in contamination from crucible. However, this

problem can be overcome perfectly if the material of crucible is the same as evaporated charge.

However, E-beam evaporation has its disadvantages: the electron beam used to heat the center of the charge may cause emission of secondary electrons that may impinge on the substrate with enough energy to produce heating or bombardment damage.

Sputtering

For thermal evaporation deposition, the source material has to be heated to a high temperature where it has high enough vapor pressure. However this method is not practical for some source material with low vapor pressure since it is difficult to find suitable crucible under such high temperature. Sputtering is an alternative method of deposition that overcomes the problem mentioned above. As shown in Figure 2-4, in sputtering, a beam of inert-gas ions is generated by one or several ion guns. Such inert-gas ions are accelerated to energies of a few kV and are directed to hit the target, which is the source material. The atoms or molecules of source material are ejected from the target due to momentum exchange from the incident ion flux. As a result, source material flies to and deposits on the surface of a substrate to form a thin film.

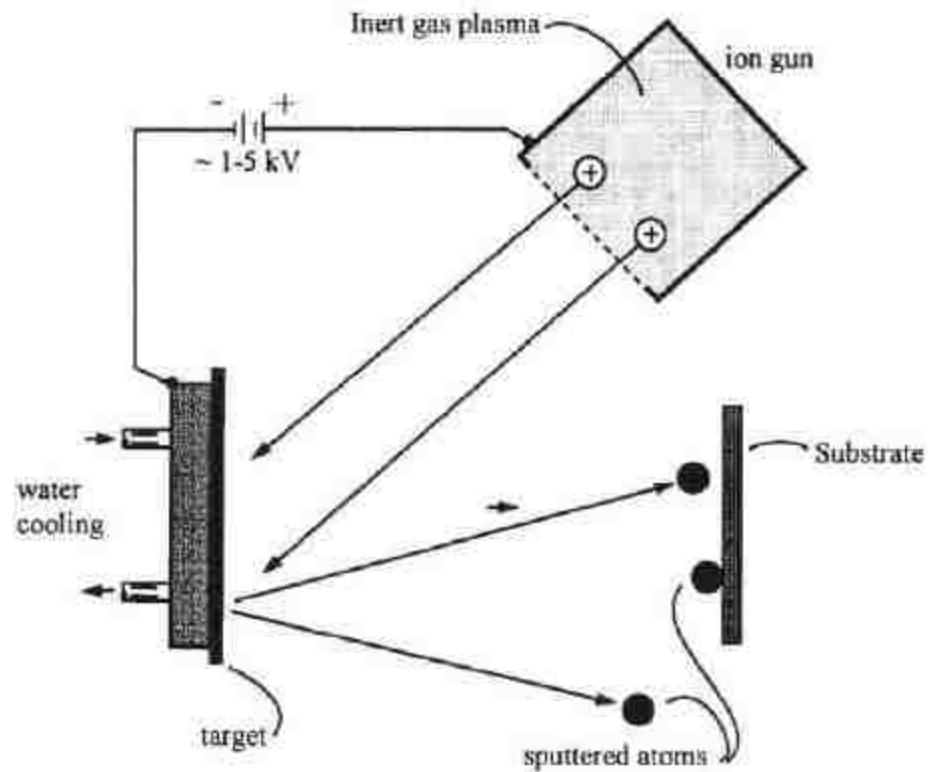


Figure 2-4 Ion beam sputtering system

Sputtering deposition has a number of advantages compared to thermal evaporation. First, the power radiated to the substrate is much less than thermal evaporation, since the temperature of target just slightly rises in sputtering. Second, sputtering does not need to evaporate source material so it can be done in a low temperature environment. Such feature gives sputtering a boarder applicable range. It can be used for almost all materials which can be used in thermal evaporation. Furthermore, compounds and alloys are not suitable for thermal evaporation if the vapor pressure of components differs widely. This is because maintaining stoichiometry will be challenged by competing partial pressure effects. However, sputtering can be used for such materials since it does not deal with evaporation. After a short time to reach steady state, sputtering

flux will have the same composition as the source target. Third, deposited atoms have higher kinetic energy, which means they have higher mobility. Such high mobility improves step coverage and enhances the quality of the thin film. Fourth, sputtering can produce much more useful deposition rate. This is especially important for refractory metals, for which evaporation rate is quite low.

However, compared to evaporation, sputtering also has several disadvantages. First, sputtering requires highly purified inert gas to avoid contamination of the film. This typically means more expensive. Second, there would be ion bombardment damage of the substrate if ion inert gas has energy level higher than 50 eV. Third, impurities within the fixture may also be incorporated into thin films.

2.1.2 Chemical Deposition

Chemical Vapor Deposition

Chemical vapor deposition (CVD) is another method of thin film growth. The reacting gas species deposit on the heated surface of substrates and chemical reactions occur to produce a solid thin film on the surface of substrates. For example, the pyrolysis of silane can be used to deposit Si films:



Typically, this reaction is used in LPCVD (low-pressure CVD) systems, as shown in Figure 2-5. The system is typically operated at ~1100 K and 1-10 Torr; deposition rate can reach 10 – 20nm/min. The LPCVD process produces layers with excellent uniformity

of thickness and material characteristics. This process is usually used to generate polycrystalline Si for integrated circuits.

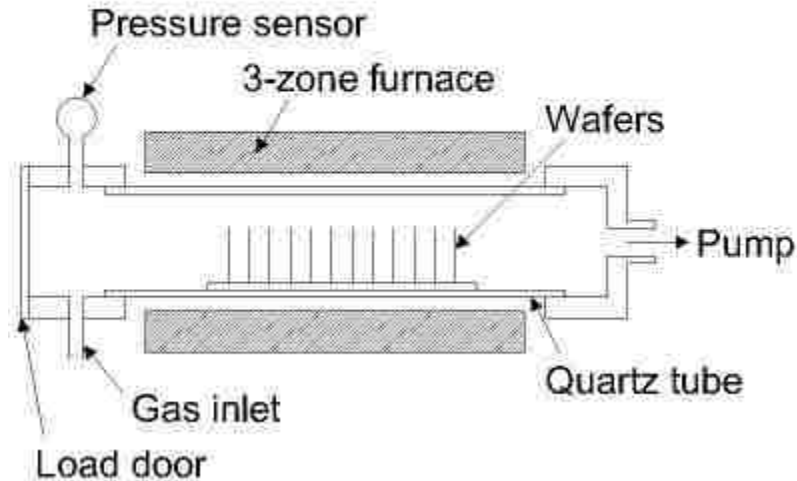
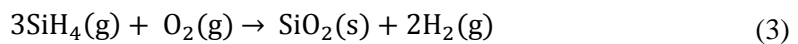


Figure 2-5 Typical hot-wall LPCVD reactor

Another CVD reaction used to generate dielectric films, e.g. silicon dioxide, is



Again, this CVD reaction system is prevalent in CVD thin film growth for integrated circuits. Furthermore, CVD provides a solution for generating refractory metal thin films.

For instance, the following reaction can be used to generate tungsten (W) thin films.



Given that the melting point of tungsten (W) is 3695 K and this CVD process typically operates at temperature much less than the melting point of tungsten (W), it can be seen why the CVD process is superior for refractory thin film deposition.

Electrodeposition

Electrodeposition is also known as “electroplating” and is typically restricted to electrically conductive materials. It is a plating process in which metal ions in a solution are moved by electric field to coat an electrode. The electrodeposition process is well suited to make films of metals such as copper, gold and nickel. The films can be made in any thickness from $\sim 1 \mu\text{m}$ to $>100 \mu\text{m}$.

In electrodeposition process, as shown in Figure 2-6, the substrate is placed in a liquid solution (electrolyte). When an electrical potential is applied between a conducting area on the substrate and a counter electrode in the liquid, a chemical oxidation-reduction reaction takes place resulting in formation of a layer of material on the substrate and usually some gas generation at the counter electrode. The voltage can be constant or is turned off and on to achieve pulsed plating. For example, in sulfuric acid solution, copper is oxidized at the anode to Cu^{2+} by losing two electrons. The Cu^{2+} associates with the anion SO_4^{2-} in the solution to form copper sulfate. At the cathode, the Cu^{2+} is reduced to metallic copper by gaining two electrons. The result is the effective transfer of copper from the anode source to a plate covering the cathode.

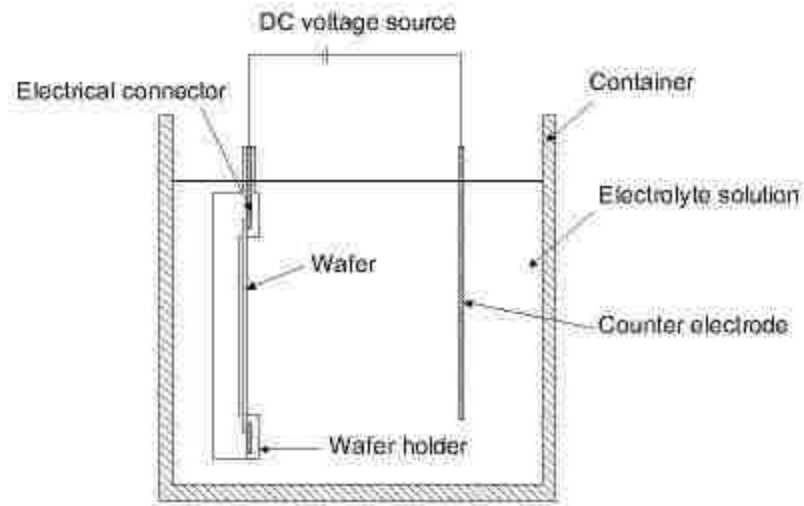


Figure 2-6 Typical setup for electrodeposition

The plating is most commonly a single metallic element, not an alloy. However, some alloys can be electrodeposited notably brass and solder. To control film thickness and uniformity, electrodeposition bath additives can be used. For instance, levelers are compounds that promote uniform surface growth. They act by attaching at asperities on the growing film and reducing the local electric field. These additives can incorporate as impurities in a growing film.

2.1.3 Comparison of Typical Thin Film Deposition Technology

There are many thin film deposition technologies used in the laboratory and industry. This is because no single technology can cover all the thin film materials and meet various requirements of thin film applications. Each of them has its advantages and disadvantages. Table 2 compares typical thin film deposition technologies and lists their features in applicable material range, uniformity, grain size and so on.

	Thermal Evaporation	E-beam Evaporation	Sputtering	LPCVD	Electrodeposition
Material	Metal or low melting-point materials	Both metal and dielectrics	Both metal and dielectrics	Mainly Dielectrics	Electrically conductive materials
Uniformity	Poor	Poor	Very good	Very good	Good
Impurity	High	Low	Low	Very low	Low
Grain Size	10 ~ 100 nm	10 ~ 100 nm	~ 10 nm	1 ~ 10 nm	10 ~ 100 nm
Film Density	Poor	Poor	Good	Excellent	Good
Deposition Rate	1 ~ 20 Å/s	10 ~ 100 Å/s	Metal: ~ 100 Å/s Dielectric: 1 ~ 10 Å/s	10 ~ 100 Å/s	10 ~ 100 Å/s
Substrate Temperature	50 ~ 100 °C	50 ~ 100 °C	~ 200 °C	600 ~ 1200 °C	20 ~ 50 °C
Directional	Yes	Yes	Some degree	Isotropic	Isotropic
Cost	Very low	High	High	Very high	Low

Table 2 Comparison of Typical Thin Film Deposition Technologies

2.2 Thin Films Growth Modes

Because thin films are widely used in electronic industry, the growth of thin films has been studied increasingly since the 1970s. Scientists and researchers use a wide range of analytical techniques, including transmission electron microscopy (TEM), scanning electron microscopy (SEM), low-energy electron microscopy (LEEM), reflection high-energy electron diffraction (RHEED), medium-energy electron diffraction (MEED), spot profile analysis low-energy electron diffraction (SPALED) and scanning tunneling microscopy (STM); with such techniques, the goal is to detect the behavior of growing material during the growth of thin films[5, 6]. At the same time, theory and computational simulations are also used in studying and understanding fundamental

phenomena controlling thin film growth. A summary of thin film growth modes based on surface energies theorem is presented below.

Most thin film growth experiments observe one of three different growth modes. A decisive period of thin film growth is the nucleation at the very early stages of the growth. The mechanisms of these three growth modes are still not well understood. However, it is widely accepted by researchers that the equilibrium shape of nucleation depends on the magnitudes of the respective free surface and interface energies. Depending on such factors three different modes of film growth are distinguished.

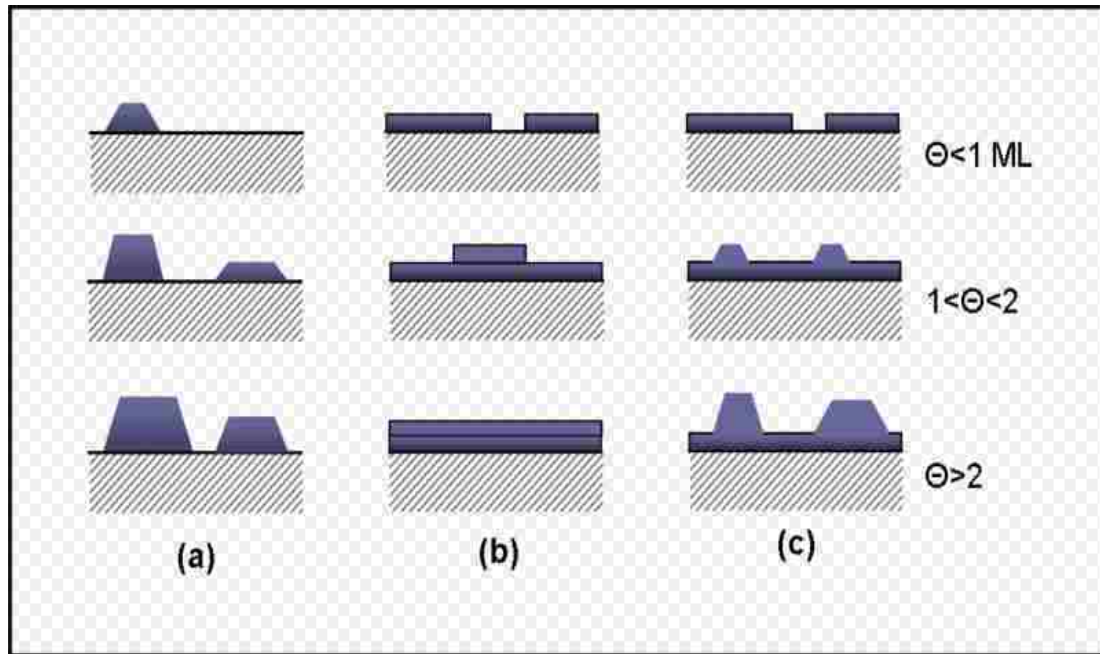


Figure 2-7 Cross-section views of the three Primary modes of thin film growth including (a) Volmer-Weber, (b) Frank-Van der Merwe, and (c) Stranski-Krastanov. Each mode is shown for several different amounts of surface coverage Θ .

(1) Volmer-Weber mode. This is also known as “3D island growth mode”. In Volmer-Weber (V-W) growth mode, atoms deposit on favored sites of substrate and form initial islands. As atoms continuously deposit on the substrate, they attach to existing

islands, which grow larger until neighboring islands start to merge or coalesce together. After initial islands coalesce, depositing atoms fill channels and voids between islands. The thickness of the continuous film does not increase until depositing atoms fill up the channels between islands and a flat film surface is formed.

(2) Frank-Van der Merwe mode. In this growth mode, atoms wet the entire surface of the substrate at the very beginning and the film grows in a layer by layer fashion. This growth mode can be viewed as “2D island growth mode”. It goes through network stage, fills in remaining 2D channels and then forms a continuous layer before growing the next layer. These are analogous steps to what are seen in 3D Volmer-Weber mode.

(3) Stranski-Krastanov mode. This growth mode occurs through a combination of Frank-Van der Merwe and Volmer-Weber mode. Stranski-Krastanov growth mode follows two steps: initially, complete films, up to several monolayers’ thick, grow in a layer by layer fashion on the surface of substrate. Beyond a critical layer thickness, growth continues through the nucleation and coalescence of discrete islands in an island growth mode.

The formation of three different growth modes can be explained by chemical potential of the first few deposited layers. Markov[7] has proposed a model for the layer chemical potential per atom as:

$$\mu(n) = \mu_B + [\varphi_a - \varphi'_a(n) + \varepsilon_a(n) + \varepsilon_e(n)] \quad (5)$$

Where n is the number of atoms, $\mu(n)$ is the chemical potential of deposited atoms, μ_B is the bulk chemical potential of the adsorbate material, φ_a is the desorption energy of an adsorbate atom from a wetting layer of the same material, $\varphi'_a(n)$ is the desorption energy of an adsorbate atom from the substrate, $\varepsilon_d(n)$ is the per atom misfit dislocation energy, and $\varepsilon_e(n)$ is the per atom homogeneous strain energy. In general, the values of φ_a , $\varphi'_a(n)$, $\varepsilon_d(n)$, and $\varepsilon_e(n)$ depend in a complex way on the thickness of the growing layers and lattice misfit between the substrate and adsorbate film. In the limit of small strains, $\varepsilon_d(n)$ and $\varepsilon_e(n) \ll \mu_B$, the criterion for a film growth mode is critically dependent on $d\mu/dn$.

In Volmer-Weber growth, $d\mu/dn < 0$. This can be viewed as that: adatom-adatom interactions are stronger than those of the adatom with the surface, leading to the formation of three-dimensional adatom clusters. During Frank-Van der Merwe growth, $d\mu/dn > 0$. This can be understood as that: adatom-adatom interactions are weaker than those of the adatom with the surface, so atoms attach preferentially to surface sites resulting in atomically smooth, fully formed layer. Stranski-Krastanov growth is an intermediary process between Volmer-Weber growth and Frank-Van der Merwe growth. In Stranski-Krastanov mode, while initial growth followed Frank-Van der Merwe mode, the chemical potential changes in sign when layer thickness reaches a critical value. This is driven by the strain terms. At this point, it is energetically favorable to nucleate islands and further growth occurs by a Volmer-Weber type mechanism.

In this thesis, focus is placed on the V-W growth mode. Many materials grow via this mode including silver (Ag), gold (Au), iron (Fe), copper (Cu), and chromium (Cr).

Furthermore, as mentioned above, similarities exist between the various growth modes so understanding one mode should help in understanding others.

In Volmer-Weber growth, intrinsic stress behavior within the thin films is complicated. The thin films are first in a compressive stress state during the nucleation and discrete islands growth stage. However, large tensile stress is observed when neighboring islands start to impinge together to form a continuous film. The films change from compressive stress stage into tensile stress stage. The phenomenon of such dramatic change in intrinsic stress is not well understood by people. In this thesis, numerical research is spent to elucidate evolution of stress behavior during Volmer-Weber growth of Au thin film and atomic scale mechanisms responsible for the stress evolution observed.

2.3 Stresses Evolution in Thin Films

This section reviews fundamental mechanisms that can generate intrinsic stresses during the growth of Volmer-Weber thin films. Based on thin film deposition experiments, the thin film growth evolution in Volmer-Weber growth mode has three morphological stages: nucleation and growth of discrete islands; coalescence of islands and formation of grain boundaries; and thickening of the continuous film. Each morphological stage during V-W growth has associated with it a stage of intrinsic stress evolution. Compressive stress is generated in the initial discrete island stage; then tensile stress rises rapidly during island coalescence and grain growth. Finally, compressive stress is created during deposition on continuous thickening films. Such phenomenon is

known as compressive-tensile-compressive (CTC) stress evolution behavior and the specific CTC behavior exhibited by a given material is known to depend on the atomic mobility of the deposition species on the substrate. Examples of force per unit width evolution during deposition of high and low mobility materials are shown in Figure 2-8. More details will be explained in the following sections, however note that what measured in stress evolution is stress-thickness product, having the unit of force per unit width (N/m). There are two kinds of Volmer-Weber growth depending on the property of thin film material itself. In low-mobility Volmer-Weber growth mode, which occurs, for instance, when deposition is done at temperature significantly below the growing film material's melting point ($T/T_m < 0.2$), the thin film remains in tensile stress state after coalescence. In other words, low mobility materials show only the compressive-tensile evolution. However in high-mobility Volmer-Weber growth mode, which occurs at higher temperature relative to T_m , complete CTC stress behavior is observed. The magnitude of such intrinsic stresses in as-deposited thin films can be well in excess of the typical yield stresses of the corresponding materials in their bulk form. Such high level stress can lead to severe problems, such as film cracking, peeling, buckling and surface roughening. Understanding the mechanisms that dictate the formation and evolution of film stress and developing strategies to control these stresses represent some of the most important outstanding issue in the thin film deposition field.

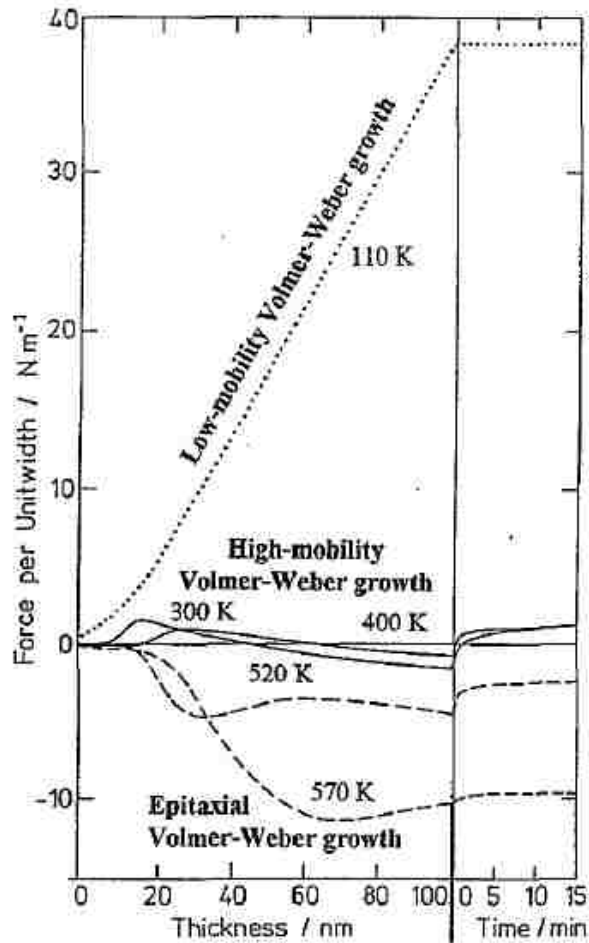


Figure 2-8 Film forces per unit width against mean thickness (left-hand side) and time (right-hand size) of Ag films UHV deposited onto mica(001) at various substrate temperatures. By convention positive and negative values denote tensile and compressive forces, respectively.

Despite many experimental investigations there is still debate over the atomic-scale mechanisms that generate intrinsic stresses. A summary and comparison between different residual stress models in Volmer-Weber thin films are presented in the following section.

2.3.1 Compressive Stress in the Discrete-Island Regime

A prevalent thought in the literature asserts that surface stress has a significant contribution to the stress evolution within a discontinuous thin film during deposition[8]. Atoms at a free surface have a bonding environment different from that of atoms in bulk phase. Such difference generates surface stresses. In other words, the bulk of the solid can be treated as applying an additional stress on the surface atoms in order to keep those atoms in atomic registry with underlying lattice. Surface stress can be understood in terms of elastically straining a free surface by a reversible amount of work. The relationship is given as

$$dW = Afd\varepsilon \quad (6)$$

where W is reversible work, A is the area of free surface, ε is strain and f is defined as surface stress. An analogous interfacial stress can be defined for the interface separating two solid phases e.g. a film-substrate interface.

Consider a case of a cylindrical island of initial height h and radius r on a substrate whose thickness is much larger compared with the size of the island. The effects of surface stress on the generation of the intrinsic stress during island growth can be based on the following two effects. First, a surface stress acts on an unconstrained island, inducing a different equilibrium lattice parameter in the island compared to that of bulk. Second, when the growing island reaches a critical size, bonding between islands and substrate becomes sufficient such that the island becomes rigidly attached to the substrate. At this point, the island is subjected to a biaxial internal stress[9] of

$$\sigma = -\frac{(f_1 + f_2)}{h} - \frac{\beta f_3}{r} \quad (7)$$

where $\beta = (1 - 3\nu)/(1 - \nu)$, ν is the Poisson ratio, f_1 is the surface stress associated with the free surface of the island, f_2 is the island/substrate interfacial stress, and f_3 is the surface stress associated with the cylindrical perimeter of the island. It is important to note here that even though the island suffers a biaxial internal stress, the entire island system is in a mechanical equilibrium state since the surface stress balances the internal stress. As such, the island induces no force (i.e. stress) on the underlying substrate. Island growth beyond this point is subject to the constraint that the island is now rigidly bonded to the substrate; that is, the island's layer of atoms closest to the substrate can no longer relax freely but is instead constrained in plane to the initial island size lattice parameter. If the island grows to a new height h' and radius r' , the lattice constant within an unconstrained island would relax to a larger value due to decreased compression from surface stress effects. However the island is rigidly attached to the substrate, the lattice parameter close to the substrate interface remains at the value appropriate to the critical island size. Island atomic layers farther from the substrate are less constrained such that a gradient in lattice parameter develops. The different lattice parameters cause a misfit strain associated with an internal stress

$$\sigma = (f_1 + f_2) \left(\frac{1}{h'} - \frac{1}{h} \right) + \beta f_3 \left(\frac{1}{r'} - \frac{1}{r} \right) \quad (8)$$

In the case where $(f_1 + f_2)$ and βf_3 are both positive (i.e. a typical situation for FCC metals), for any island with (f', r') bigger than (f, r) , the internal biaxial stress is negative, which means that the internal stress is compressive stress. The prediction of this

surface stress model is consistent with experimental measurements. Nonetheless, it is also widely argued that this model cannot explain all existing data. For example, this model does not explain what determine critical size and does not supply a solution to calculate critical size. What is more, this model does not explain detailed atomistic interaction on island/substrate interface. For example, the assumption the atoms closest to the substrate become rigidly locked into a certain lattice constant is widely considered suspect.

2.3.2 Tensile Stress in the Island-Coalescence Regime

The second stage of V-W growth is when growing islands impinge on one another and coalesce. During this growth stage, tensile stress typically emerges, sometimes to very significant magnitude. Theories explaining tensile stress evolution invoke the picture that two free surfaces snap together to form a grain boundary when growing islands impinge. This eliminates surface energy at the expense of generating (tensile) elastic energy. Such rapid tensile rise is correlated to two processes: 1) island coalescence to form grain boundary, and 2) grain growth. Several models for calculating the tensile stress during islands coalescence process are reviewed here.

Hoffman et al. first suggested that tensile stress was generated when two neighboring discrete islands impinge on each other[10]. In such case a grain boundary was assumed to form and two free surfaces were eliminated driven by a tradeoff between surface energy and elastic energy. In his analysis, cubic islands with parallel vertical free surfaces grow on a flat substrate and two neighboring islands snap together when the distance between them becomes a critical value. The stress calculated by this model is given as

$$\sigma = \sqrt{\frac{M(2\gamma_s - \gamma_{GB})}{w}} \quad (9)$$

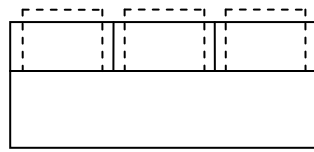
where γ_s and γ_{GB} are free surface energy and grain boundary energy, respectively, w is the grain size and M is $E/(1-\nu)$. In coalescence process, free surface energy reduction is balanced by strain elastic energy increase which is consistent with a reversal of Griffith's criterion for crack propagation – the crack will only advance if the elastic energy reduction is greater than the surface energy increase from creating two free surfaces. However, if one assumes typical values $(2\gamma_s - \gamma_{GB}) = 2 \text{ J/m}^2$, $M = 100 \text{ GPa}$, $w = 500 \text{ \AA}$, equation (9) above leads to a stress estimate of $\sigma = 2 \text{ GPa}$, which is much larger than observed experimental value. This approach can also produce an expression for the gap size between two islands that will be eliminated by coalescence of the islands. Again, using typical values for relevant parameters, one obtains gap size that is much larger than what is observed in experiments.

Nix and Clemens[11] developed a more sophisticated model that treats boundary formation as a crack-closure process. They considered hemisphere shape islands on a flat substrate and in the initial contact of islands, the adjacent free surfaces join together to form a “crack”. The “crack” closes rapidly by pulling two free surfaces together to form a grain boundary.

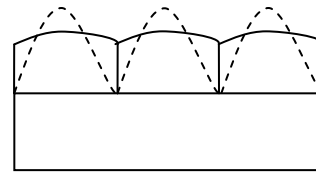
Freund and Chason[12] developed a more realistic geometry model for explaining tensile stress evolution in thin films. They suggested a cohesive attraction between two adjacent surfaces as a major driving force for islands coalescence. The volume-averaged stress that develops in the island array can be written in the form

$$\left\langle \frac{\sigma^{(N)}}{E} \right\rangle = A_N \left(\frac{2\gamma_s - \gamma_{GB}}{2rE} \right)^{C_N}, N = 1, 2, 3 \quad (10)$$

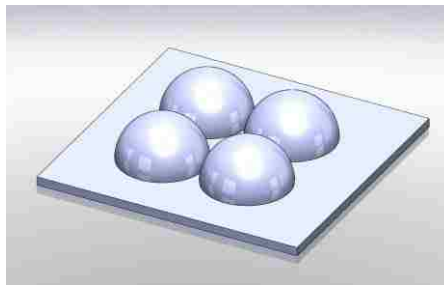
Where E is Young's modulus, N corresponds to the dimensionality of the model, C_N is an exponent that depends on the system dimension ($C_1=1/2$, $C_2=2/3$, $C_3=1$) and A_N is a numerical factor ($A_1 = 0.82$, $A_2 = 0.44$, $A_3 = 4$). When $N = 1$ and $N = 2$, the above equation gives the same results as Hoffman's model and Nix-Clemens model, respectively. Figure 2-9 shows this model in one, two and three dimensions.



(a) Hoffman (N=1)



(b) Nix-Clemens (N=2)



(c) Freund-Chason (N=3)

Figure 2-9 Views of (a) coalescence geometry used in Hoffman's analysis, (b) coalescence geometry used in Nix and Clemens's analysis, and (c) coalescence geometry used in Freund and Chason's analysis. Dashed lines in (a) and (b) represent the shape of islands just prior to coalescence.

Considering three dimension geometry, the estimate of tensile stress of the equation above gives magnitudes consistent with experiments for high-mobility metal thin films. However, for low mobility metals, stress value observed in experiments is

significantly higher than the estimate from Nix-Clemens ($N=2$) and Freund-Chason ($N=3$) model. For low mobility materials, the magnitude of stress is more consistent with the $N = 1$ case. In addition, these first models of coalescence stress generation only considered stress generated when islands initially coalesce. They did not address tensile stress that evolved after initial coalescence.

Sheldon et al. proposed a combined approach to coalescence stress using a cohesive zone approach along with a finite element model that accounts for a faceted morphology[6]. He considered that there are steps in the cohesive zone and each step suffers constraints from underlying strained step. The process of steps closing up can be viewed as the process of free surface coalescence and boundary formation. Additional tensile stress develops as each set of steps coalesces or zips together. This model assumed that coalescence is driven by short-range attraction, and therefore avoids unphysical prediction of stress magnitude. This model explains tensile stress that has been observed to continue increasing significantly after thin films become continuous in low-mobility films. Indeed, it is now common to distinguish between initial coalescence stress and ongoing coalescence stress.

Another mechanism frequently discussed for tensile stress is grain growth. Polycrystalline films are comprised of many crystallites or grains. For instance, two discrete islands can eventually grow to become neighboring grains. It is important to note that the atomic number density is lower near a grain boundary area, compared to the bulk. As grains growing, the grain boundary area decreases and the density of the whole film increases correspondingly. This would normally drive lateral contraction of a film;

however contraction is constrained by the underlying substrate. This induces tensile stress in the film. The connection between tensile stress and grain growth[13] can be expressed as

$$\sigma_{GG} = 2M\Delta a \left(\frac{1}{D_0} - \frac{1}{D} \right) \quad (11)$$

where Δa is the excess free volume per unit area of grain boundary, and D and D_0 are the instantaneous and as-deposited grain diameters, respectively. Such an expression includes a parameter Δa that is not easily obtained from experiments. Nonetheless, experimental data can be fit to produce a value for Δa and such value appears reasonable.

2.3.3 Postcontinuity Compressive Stress

In Compressive-tensile-compressive (CTC) stress evolution behavior, after islands coalescence and form a continuous film, tensile stress is observed to drop back to compressive stress in high mobility films. Low mobility materials typically remain tensile, though some amount of compression may evolve. Note that atomic mobility on a surface is determined by the interaction strength between the adatom and the existing surface, relative to the ambient thermal energy given by kT , where k is Boltzmann constant and T is absolute temperature.

Two generic mechanisms are frequently discussed for the origins of compressive stress during the final V-W growth stage[4, 9]. One of them is the surface stress mechanism discussed in discrete islands stage of V-W film growth. In this case, when islands initially coalesce they have a certain size and lattice parameter. As films thicker, island height increases so islands are increasing in size. This means surface stress effects

are smaller such that an unconstrained island would relax to a larger lattice constant. However, in the final stage of V-W growth lateral island relax is constrained by neighboring grains, or islands. Thus, compressive stress develops. The magnitude of stress associated with surface stress mechanism has been estimated as

$$\sigma(h) = \sigma_0 - (f_1 + f_2) \left(\frac{1}{h_0} - \frac{1}{h} \right) \quad (12)$$

where σ_0 is the initial tensile stress after islands coalescence, h_0 is the film thickness with tensile stress σ_0 and h is as-deposited height of continuous film after film reach h_0 thickness. Depending on the magnitude of σ_0 , the film can return to compressive stress stage during growth. However the surface stress mechanism cannot explain a commonly observed reversible relaxation phenomena: a rapid relaxation of compressive stress occurs when growth is interrupted; but upon resumption of growth, this relaxation is fully reversed and the same compressive stress is reestablished.

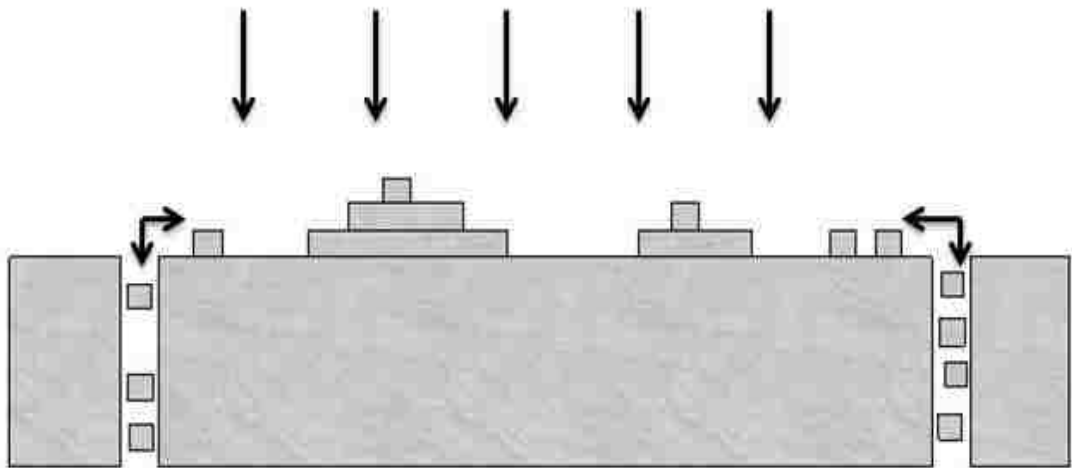


Figure 2-10 Schematic of model for flow of atoms into, and out of the grain boundaries by change in surface potential

To explain reversible relaxation phenomena, another mechanism was proposed by Chason and Sheldon[4]. As shown schematically in Figure 2-10, such a mechanism is based on excess atoms entering grain boundaries, driven by the increase in surface chemical potential associated with deposition flux. As atoms deposit on a film surface, chemical potential of film surface is greater than that in grain boundary. Such difference in chemical potential drives excess atoms from the growth surface into grain boundary to generate compressive stress. This flow of excess atoms into grain boundary continues until resultant compressive stress increases chemical potential in grain boundary to equal that on growing surface; at that point, a steady state is achieved. When deposition flux is terminated, the chemical potential of surface drops and excess atoms are driven out of the grain boundary and back to the growth surface, decreasing the compressive stress. After the deposition flux is resumed, the same process described above is reestablished, increasing the compressive stress as observed. This model can explain reversible relaxation phenomena observed in final stage of V-W growth; what is more, it also brings the view that how compressive stress can be created within grain boundaries.

2.4 Stresses Measurement and Analysis Technology

Many methods are used to measure and study intrinsic stresses within thin films. Most of them can be categorized into two classes: techniques that measure the bending of substrates to determine film stresses and diffraction methods e.g. x-ray diffraction and LEED (low-energy electron diffraction)[14-20].

Considering substrate deformation based methods, stress arises when the film undergoes any dynamic microstructural evolution process that changes the density of the film while the film is rigidly attached to its substrate. The substrate undergoes a slight bending resulting from the forces and moments imposed by the film. By measuring the substrate bending one can determine intrinsic stress in the film. While substrate bending negligibly relieves the strain in the film, the substrate curvature provides a very useful means of measuring the film stresses. To ensure this is true, a substrate significantly thicker than the film must be used. The substrate curvature and film stress can be correlated by the Stoney equation[21]

$$k = \frac{6\sigma h}{M_s h_s^2} \quad (13)$$

where k is the substrate curvature, σ is the mean in-plane biaxial film stress, h is the film thickness, M_s is the biaxial elastic modulus of the substrate and h_s is the substrate thickness. There are two ways to determine the substrate curvature. One is measuring the change of the reflection angle of a laser beam; the other is detecting substrate displacement through capacitance methods. Typically, the stress-thickness product (σh) is plotted versus thickness, as shown in Figure 2-8. Thus the derivative of σh with respect to h gives the instantaneous stress in the film (i.e. the stress in the currently deposited layer). On the other hand, the total σh divided by total h gives the volume average stress in the film.

In addition to substrate curvature techniques, diffraction techniques, e.g. x-ray diffraction, LEED (low-energy electron diffraction), MEED (medium-energy electron diffraction), are used to detect film intrinsic stresses. For example in x-ray diffraction, the

strain in the crystal lattice is directly measured by measuring the atomic inter-planar spacing. Then residual stress that produces the strain is calculated by assuming a linear elastic distortion of the crystal lattice. Diffraction techniques are more difficult to implement *in situ* (i.e. during growth). Nonetheless, notable advances for *in situ* analysis via diffraction based methods have been made.

Chapter 3 Numerical Procedure

3.1 Numerical Simulations

Computer simulation is the discipline of designing a model of an actual or theoretical physical system, executing the model on a digital computer, and analyzing the execution output. Computer simulation was first pioneered as a scientific tool in the period of World War II, but it has grown rapidly to become indispensable in a wide variety of scientific disciplines. In engineering, computer simulations are widely used in the realm of thermal transport, fluid flow, and stress analysis. Computer simulation acts as a bridge between theory and experiment: having characterized a physical system in terms of model parameters, simulations are often used both to solve theoretical models beyond certain approximations and to provide a hint to experimentalists for further investigations. One can test a theory by conducting a simulation using the same model; one can also test experiments by comparing data from simulations and experiments; one can even conduct a simulation to unveil phenomena that are difficult or perhaps impossible to be observed in experiments.

There are different types of computer simulations with different accessibility of time and length scale[22]. A not surprising trend is that more detailed methods– as far as the physical degree of freedom resolved – are unable to access long time and large length scales. Figure 3-1 shows regions of time and length scales for different types of simulations.

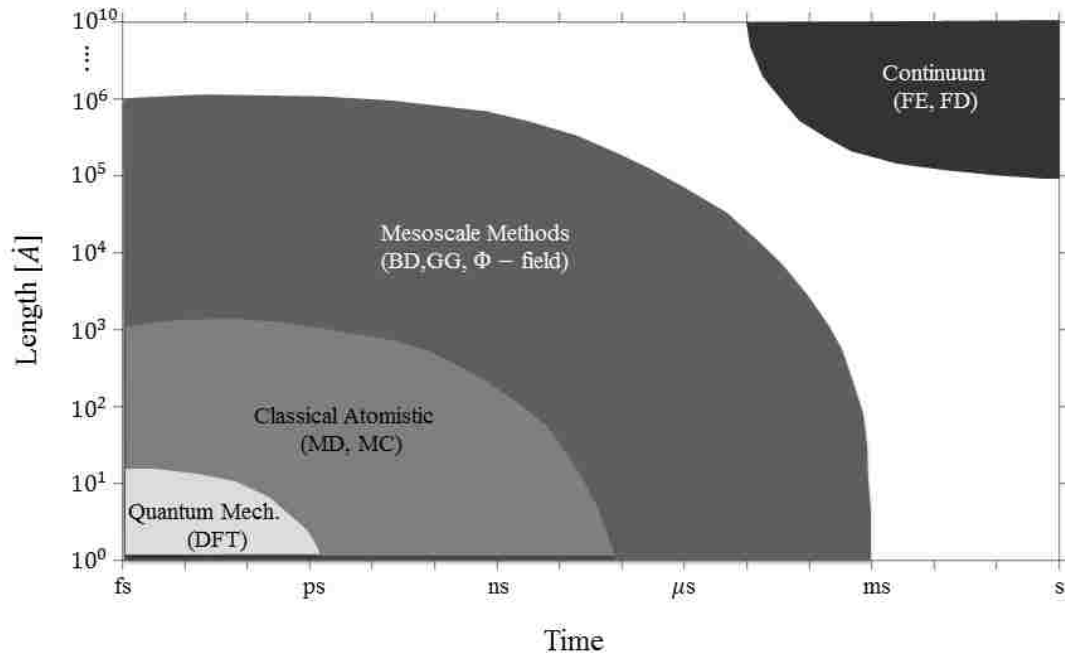


Figure 3-1 Schematic comparison of time- and length-scales, accessible to different types of simulation techniques (quantum mechanics (DFT), classical atomistic (MD, MC), mesoscale methods and continuum (FE, FD))

It is clear from Figure 3-1 that quantum simulations in which fast motions of electrons are explicitly taken into account has typical length and time scale of order of Angstroms (\AA) and picoseconds (ps), respectively. Classical molecular dynamics (MD) approximates electron motions in a coarse-grained fashion (i.e. via an atomic force field), and is dominated by the time of interatomic or intermolecular collision events, rotational motions or intramolecular vibrations. As such, MD has accessible time scale of order nanoseconds (ns) and length scale of order 10 – 1000 \AA . Mesoscale methods coarse grain physical systems further, no longer explicitly resolving atoms. For example, Brownian Dynamics (BD) is a simplified version of Langevin dynamics and corresponds to the limit where no average acceleration takes place during the simulation run. It is usually used to trace particles in a solvent medium, thus both atoms and electrons are represented

in coarse grain fashion. As a result, its typical length and time scale can reach 10 – 1000 nm and microsecond (μs). If one is not interested in microscopic resolution of a system, but can instead describe a system via average, macroscopic quantities, continuum methods may be applied. For example, methods based on the finite element formalism represent materials in term of their known thermomechanical properties. They are therefore able to address large length scale of meters to kilometers and time scale from milliseconds (ms) to years.

3.2 Molecular Dynamics Simulations

Two main families of computer simulation techniques for atomistic scale many-body systems are the Molecular Dynamics (MD) method and Monte Carlo (MC) method[22, 23]. Additionally, there are many hybrid methods that combine the features of both. Molecular Dynamics (MD) is a form of computer simulation in which atoms and molecules are allowed to interact for a period of time by approximations of known physics, giving a view of the real space, real time trajectory of the particles. MD lets scientists peer into the motion of individual atoms in a way which is not possible in most laboratory experiments.

Molecular Dynamics (MD) are based on the following governing equations,

$$m_i \ddot{r}_i = f_i \quad f_i = -\frac{\partial}{\partial r_i} \mathcal{U} \quad (14)$$

where f_i is the force acting on the atom i , r_i represents the coordinate of atom i and \mathcal{U} is potential energy of the system. It is clear that the potential energy \mathcal{U} is required to

calculate the force f_i . As stated previously, electrons are not explicitly resolved in classical atomistic simulations. Their influence on atomic bonding is described via a potential energy function that depends only on atomic positions, $\mathcal{U}(\vec{r}_i)$. The simplest such functions only consider atom pair separation distances. An example is Coulomb Law describing the interaction energy for charge containing systems. However, \mathcal{U} can be more complicated, with terms that involve groups of three, four, or more atomic positions. Many MD implementations are cast in terms of Hamiltonian mechanics wherein a systems. Hamiltonian is defined as a sum of kinetic and potential energy $\mathcal{H} = K + \mathcal{U}$. Adopting this formalism, Hamilton's equations of motion, are used:

$$\dot{p}_i = -\frac{\partial \mathcal{H}}{\partial q_i} \quad , \quad \dot{q}_i = \frac{\partial \mathcal{H}}{\partial p_i} \quad (15)$$

These equations are integrated to move atoms to new positions and get the new velocities at these new positions.

Like all computer simulations, Molecular Dynamics (MD) simulation needs appropriate inputs to reproduce or approximate experimental findings. There are three basic ingredients for a MD program:

- (1) A model describing the interaction between system constituents is needed. In the current study, for instance, the model employs a short-range interaction that has a spatial cut off of $\sim 6\text{\AA}$. This reduces the computational cost of a simulation while still providing a realistic description of metallic atomistic behavior.

- (2) An integrator is needed to propagate particle positions and velocities from time t to $t + \delta t$, where δt is the simulation time step. Note that the time step is chosen to ensure stability of the integrator.
- (3) A statistical ensemble has to be chosen, which dictates the thermodynamic state quantities like temperature and pressure that are controlled.

The three ingredients above essentially define a MD model and with such inputs, a MD program can generate data like temperature, pressure, and stress at atomic scale for every time step. Such detailed thermodynamic data are difficult to measure in experiments. Relevant to this current study, having such information from MD simulations, we can study intrinsic stress evolution behavior within thin films and atomic scale mechanisms driving it.

3.2.1 Molecular Interaction

The most accurate descriptions of atomic scale interactions – or potential energy \mathcal{U} – utilize quantum mechanical theory. That means the Schrödinger equation is used to solve the atomic scale interactions. However, to study even nanometer scale systems, one must simplify the description of potential energy to reduce computational cost. In the current study, only short-range interaction is taken into account. Specifically, crystals like metals have well defined nearest neighbor distance, second nearest neighbor distance, etc. The model used here includes interaction out to the third nearest neighbor. It offers the possibility to consider only some neighboring atoms. As such, a cut off distance is introduced and interactions between atoms beyond that cut off distance are not taken into account. Quantum mechanics confirms such an approximation is reasonable for many

materials, including metals. The reason is that, atoms at relatively closer distances screen interactions from atoms at relatively farther distances. Thus, the majority of an atom's bonding energy is dictated by its interactions with atomic neighbors in the first three neighbor distance shells. In the current study, the embedded atom method (EAM) is used in the molecular dynamics (MD) program. The EAM is an approximation describing the energy in an atomic system and it is particularly appropriate for metallic systems. The energy of an atom in an ensemble governed by the EAM interaction model can be written as

$$E_i = F_i \left(\sum_{j \neq i} \rho_j(r_{ij}) \right) + \frac{1}{2} \sum_{j \neq i} \Phi_{ij}(r_{ij}) \quad (16)$$

where r_{ij} is the distance between atoms i and j , Φ_{ij} is a pair-wise potential energy function, ρ_j is the contribution from atom j to the electron charge density at the location of atom i , and F is an embedding function that represents the energy required to place atom i into electron cloud given by $\sum_{j \neq i} \rho_j(r_{ij})$. The embedding term shows the EAM has a multibody contribution since the argument to F_i is determined by all atomic neighbors to atom i (within the interaction cut-off).

3.2.2 Integrator

The integrator is responsible for the accuracy of a molecular dynamics program once the potential interaction function is given. The integrator serves as a bridge to connect the current time step to the next time step, propagating the state of the atomic configuration (positions, velocities, etc.) from time t to $t + \delta t$, where δt is the simulation time step. A good integrator should be accurate enough to produce a trajectory

that approximates the true trajectory with high accuracy while avoiding numerical instabilities. Ideally, a chosen integrator also permits as large a time step as possible while still maintaining the desired thermodynamic ensemble.

One of the most common integrators used in molecular dynamics is the ‘velocity Verlet’ algorithm. Consider the atomic momenta $p^N = (p_1, p_2, \dots, p_N)$, then the classical equations of motion can be written as

$$\dot{r}_i = \frac{p_i}{m_i} \quad \text{and} \quad \dot{p}_i = f_i \quad (17)$$

This is a system of coupled ordinary differential equations. The ‘velocity Verlet’ algorithm performs a step-by-step numerical integration of these differential equations as following

$$p_i\left(t + \frac{1}{2}\delta t\right) = p_i(t) + \frac{1}{2}\delta t \cdot f_i(t) \quad (18)$$

$$r_i(t + \delta t) = r_i(t) + \delta t \cdot p_i\left(t + \frac{1}{2}\delta t\right) / m_i \quad (19)$$

$$p_i(t + \delta t) = p_i\left(t + \frac{1}{2}\delta t\right) + \frac{1}{2}\delta t \cdot f_i(t + \delta t) \quad (20)$$

This simple algorithm has two advantages: first, it is low order in time so it allows long timesteps; second, it calculates force only once in every time step. The force calculation can be computationally expensive, so this makes the program more efficient.

3.2.3 Ensembles

Molecular Dynamics (MD) simulations use thermodynamic ensembles to control certain thermodynamic quantities, e.g. the temperature or pressure. There are different

thermodynamic ensembles and one chooses an ensemble based on desired imposed conditions along with corresponding desired simulation output. Here the Microcanonical ensemble (NVE), Isothermal-Isobaric ensemble (NPT) and Canonical ensemble (NVT) are presented.

In microcanonical ensemble, the system maintains constant number of atoms (N), volume (V) and energy (E). It corresponds to an adiabatic process with no heat exchanger. A microcanonical molecular dynamics trajectory can be viewed as an internal exchange of potential and kinetic energy, with total energy being conserved.

In the isothermal-isobaric ensemble (NPT), number of atoms (N), pressure (P) and temperature (T) are kept constant. In such an ensemble, algorithms are required to maintain temperature (T) and pressure (P) at a user specified value. These are called a thermostat and barostat algorithm, respectively. Such an ensemble corresponds to laboratory conditions open to ambient temperature and pressure.

In canonical ensemble (NVT), number of atoms (N), volume (V) and temperature (T) are fixed. It is also sometimes called constant temperature molecular dynamics. Only a thermostat algorithm is required. A thermostat algorithm adds or removes thermal energy (i.e. atomic, non-translational kinetic energy) from the system to maintain constant average temperature. The ways to add and remove energy from the boundary of a MD system are various; in general, the algorithms act on atomic velocities to control temperature. Specific thermostat algorithms are the Nosé-Hoover thermostat, the Berendsen thermostat and Langevin dynamics thermostat. Barostat algorithms operate by changing simulation system volume to keep pressure constant.

3.3 Simulations Description

This study focuses on carrying out Molecular Dynamics (MD) simulations to elucidate stress behavior evolution at island boundaries during the growth of metal thin films. As such, this work focuses on tensile stress evolution during the second, island coalescence, stage of V-W growth. Specifically, this study examines tensile stress evolution behavior in high-mobility Volmer-Weber growth mode. The material modeled is gold (Au). Gold has a relative low melting point among metals; furthermore, its relatively inert chemical nature imparts Au atoms relatively high mobility on many substrate materials at room temperature. Au is also a face centered cubic (FCC) metal; as such, it is hoped that some general notions will be gained for high mobility FCC metals. Film growth is modeled by simulating atomic deposition onto a substrate. At the very beginning of deposition simulations, two neighboring islands on a flat substrate contact each other and generate an initial coalescence stress. As deposition goes on, a grain boundary forms as two free island surfaces snap together (i.e. ongoing coalescence). This study analyzed stress behavior during the on-going coalescence process. In on-going coalescence, some initial coalescence events were assumed to have already occurred. The simulation modeled atom deposition onto the initially coalesced islands. These two neighboring island free surfaces merged together as atoms continued depositing into the gap between islands. More will be said about simulation details below, but Figure 3-2 and Figure 3-3 show schematic representations of the configuration of the system before and after deposition simulations.

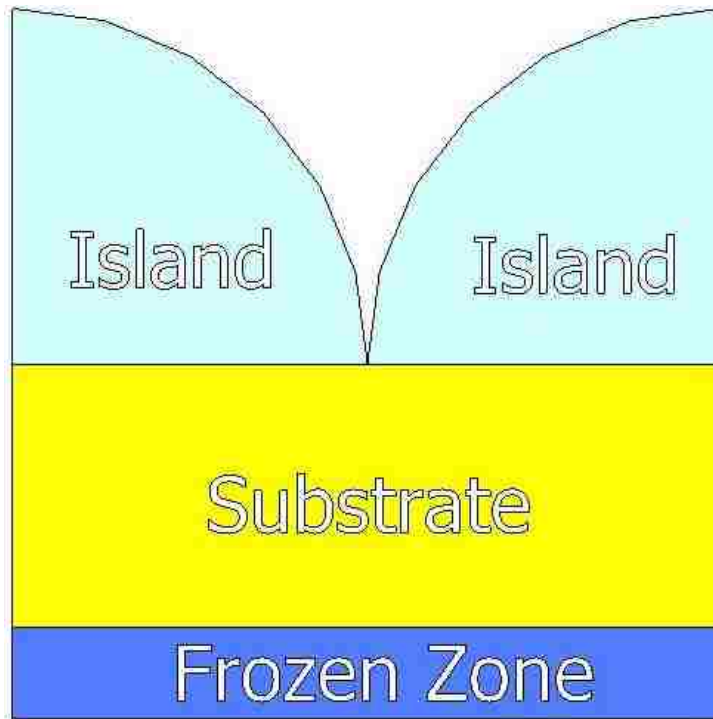


Figure 3-2 Structure of "Island-Substrate" system before deposition, including three zones: (a) frozen zone, (b) substrate, and (c) islands

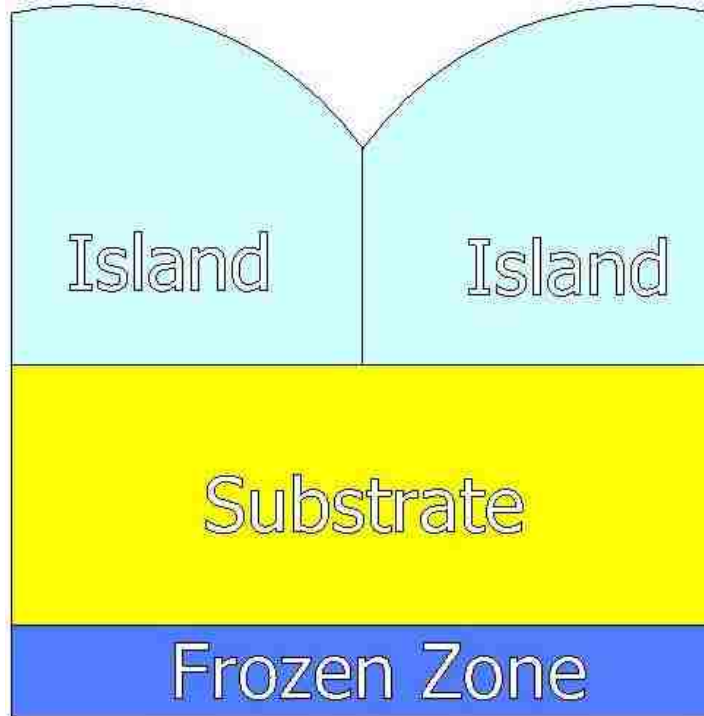


Figure 3-3 Structure of "Island-Substrate" system after deposition, including a grain boundary and three zones: (a) frozen zone, (b) substrate, and (c) islands

Temperatures of computational simulations were at $T = 300$ K. The diameter of islands was 10 nanometers. A deposition rate of 1 atom every 3000 time steps was chosen; lattice orientation was $[0\ 0\ 1]$, normal to the substrate surface. Two key parameters, deposition energy $E = 8.27 \times 10^{-3} eV$ and substrate thickness of 10 nm, were used in simulations to elucidate intrinsic stress behavior within thin films. For each simulation, five different random number seeds were used to account for stochastic variations in the deposition process. This study examines tensile stress as a function of time, the magnitude of the maximum tensile stress, evolution of each stress component and their hidden mechanisms.

The code used in this study was LAMMPS. LAMMPS is a classical molecular dynamics code and an acronym for Large-scale Atomic/Molecular Massively Parallel Simulator. There were three basic kinds of LAMMPS output:

- (1) Thermodynamic output. Thermodynamic output contained a list of quantities which was printed periodically to the screen and logfile.
- (2) Dump files. Snapshots of atoms and various per-atom values were written at a user specified frequency into dump files.
- (3) Restart files. Restart files were used to restart a program at a specified timestep and were written at a user specified frequency.

Except for those three kinds of files, another kind of file named data file was used in this study. Data files could be generated from dump files and contained general system information, e.g. simulation box size, boundary conditions, and atoms coordinate and velocity information.

3.4 Simulation Procedures

Before starting the deposition simulations, the “island-substrate” system, as shown in Figure 3-3, must be prepared. There were three steps before the deposition simulation: bulk equilibrium, creating free surfaces, and creating islands on the substrate.

The equilibrium lattice parameter for $T=300\text{K}$, $P=0$ was calculated first. The $T=0$ lattice parameter was available in input interaction potential energy file. However, it was not the correct lattice parameter for the specified temperature. In order to find out that parameter, a Au crystal was formed that was $8 \times 8 \times 8$ unit cells in x , y , z direction, respectively. Periodic boundary conditions (PBCs) were employed in x , y , z direction. This system was run in an NPT ensemble using a Nose-Hoover thermostat. Atomic velocities were initialized to represent a system temperature two times what was desired. Equipartition demands that half the energy go from kinetic to potential energy modes when the MD simulation begins. Thus, temperature dropped in half at the start of the simulation. Once the system reached $T=300\text{K}$, $P=0$, the equilibrium lattice constant was obtained from the system volume.

Once the equilibrium lattice parameter was determined, a Au crystal with size of $10 \text{ nm} \times 5 \text{ nm} \times 10 \text{ nm}$ was constructed. Two other crystals, with 15 nm and 25 nm in z direction, were also constructed. These crystals were built using the $T=300\text{K}$, $P=0$ lattice parameter. They were then run in canonical ensemble (NVT) with periodic boundary conditions in x , y , z direction. Note that the use of periodic boundary conditions in all three directions models an infinite crystal, as far as local atomic bonding environments.

However, a physical length scale for the simulation exists and is given by the total simulation cell size.

After the bulk crystals were equilibrated, free surfaces were formed at the z top and the z bottom of each simulated Au crystal. This was done by removing periodic boundary condition in z direction; care was exercised during this step to ensure no atomic planes of atoms were divided across the periodic boundary condition. The model Au crystals with free surfaces in z direction were then run for 10^4 timesteps to equilibrate the free surface structure. Canonical ensemble (NVT) and periodic boundary conditions were used in this run: however, it is not strictly a constant V ensemble since free surfaces exist.

After equilibrating the free crystal surface models, a hemi-cylindrical island was formed on the +z surface for each crystal. The hemi-cylinder was formed by deleting all atoms from the simulation whose (x, z) coordinates were such that,

$$Z > Z_C \text{ and } (X - X_C)^2 + (Z - Z_C)^2 > (5 \text{ nm})^2 \quad (21)$$

where $X_C = 5 \text{ nm}$ and $Z_C = 5, 10, 20 \text{ nm}$ for crystals with z-direction thickness of 5, 10, 20 nm, respectively. Note that, due to periodic boundary condition in y direction, this is a model of an infinite hemi-cylinder in y direction. Thus, in principle, this is a model of coalescence in the x direction under a plane strain condition. Because deposition was only modeled on the hemi-cylindrical surface (in +z direction), a slab of atoms at the flat surface (in -z direction) was held frozen. This ensured that momentum imported to the substrate during deposition did not cause the entire atomic system to drift in the z direction.

A schematic of the computational domain used to model an “island-substrate” system is shown in Figure 3-4. In x- and y-directions, periodic boundaries were used.

This implied that atoms on the $+x$ surface of the hemi-cylinder can interact with atoms on the $-x$ surface of the hemi-cylinder, through the periodic boundary in x direction. To emphasize this, the entire atomic ensemble was translated in $+x$ by an amount equal to half the simulation cell size in x direction. The periodic boundary condition in x naturally put atoms back into the simulation cell such that the gap between the hemi-cylinder free surface (in x direction) was at the center of the simulation cell. Note again: this is purely for rendering purposes; PBCs in x ensure the simulation is the same regardless of the gap position.

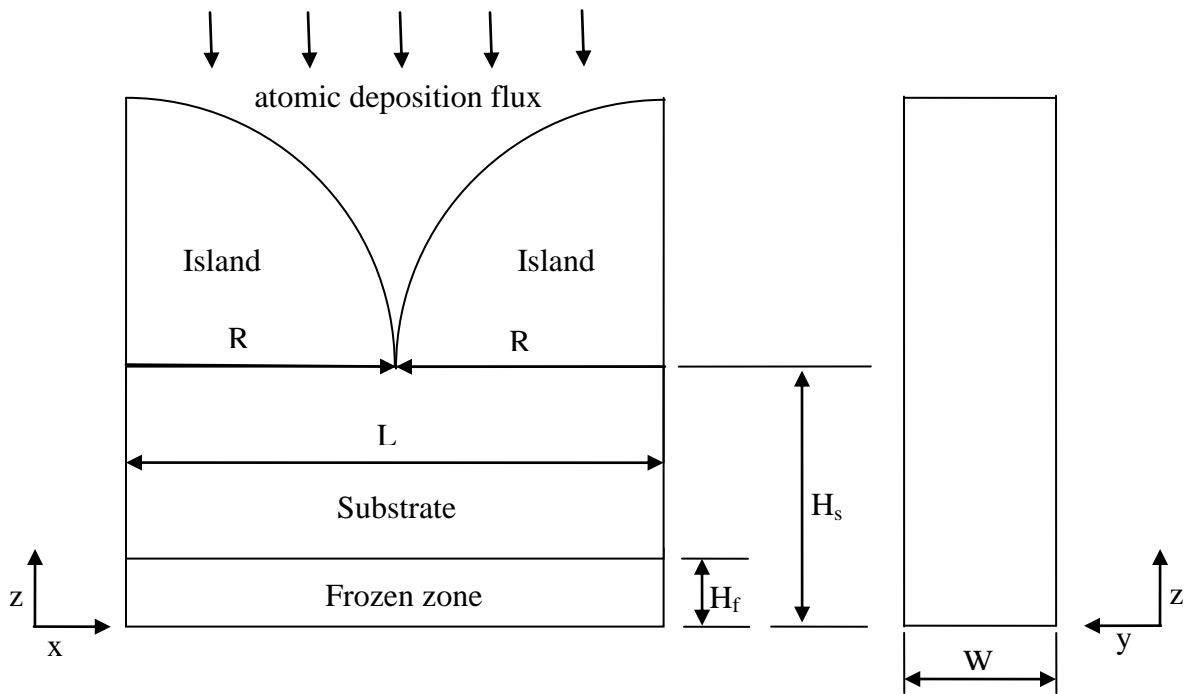


Figure 3-4 Schematic of computational domain

Figure 3-4 shows the computational domain in this study. The left part and right part are the front view and side view of the computational domain, respectively. There were three zones in computational domain: islands, substrate and frozen zone. Note that

frozen zone was considered a part of substrate. Though only one explicit island is modeled, periodic boundary condition in x direction makes this a model of an infinite array of uniform islands in x direction, as shown in Figure 3-5. The “~” sign used to stand for periodic boundary conditions. The frozen zone contained six atom layers in which those atoms were kept static; this was achieved by setting both their forces and velocities to zero. Three values of substrate thickness H_s were chosen $H_s = 5$ nm, 10 nm, and 20 nm, to compare the effects of different thickness of substrate throughout the simulation. The radius of islands was 5 nm. Table 3 summarizes the simulation parameters.

Name	Symbol	Range of values (or value)
Radius of islands	R	5 nm
Substrate thickness	H_s	5, 10 and 20 nm
Frozen zone thickness	H_f	~ 1.3 nm (six atom layers)
Simulation cell length in x direction	L_x	10 nm and ~11 nm
Simulation cell width in y direction	W_y	5 nm
Gap width	Δ	2 lattice parameters And 0

Table 3 Geometry of computational domain

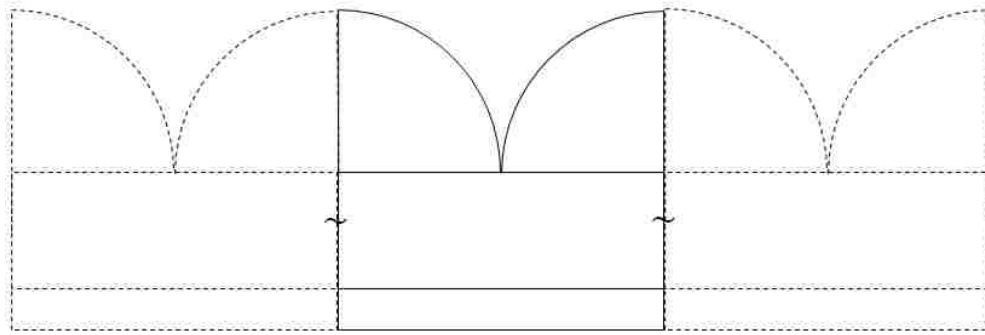


Figure 3-5 Schematic of computational domain II. Dashed line configurations indicate infinite array of uniform islands in x direction.

The system shown in Figure 3-4 had initial coalescence stress at the very beginning of the deposition simulation. This is because free surface atoms at the island-substrate interface and several atomic layers above can interact with each other. The stress created by such interaction is called initial coalescence stress. To calculate initial coalescence tensile stress, another model was prepared for comparison, as shown in Figure 3-6. Compared to the first model, this model had the same geometry but a larger length L_x in x-direction, leading to a gap between island surfaces in x direction. The gap width Δ was two lattice parameters, which was enough to prevent atoms on the island surfaces from interacting. In other words, there was no initial coalescence stress in this model.

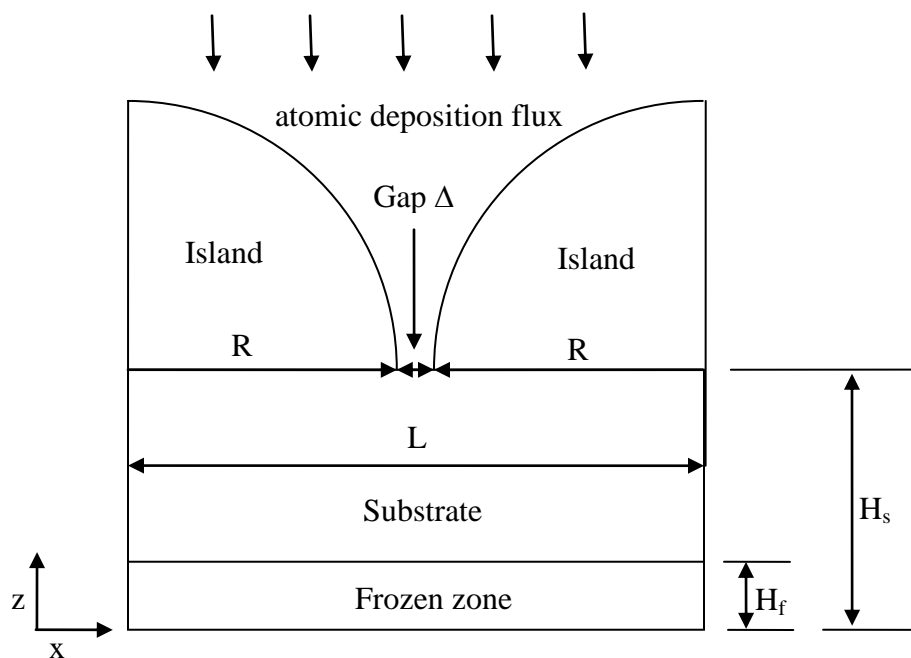


Figure 3-6 Schematic of computational domain III

As stated previously, one atom was deposited every 3000 time steps. The time step used was 0.001 picosecond (ps) throughout. Thus, the deposition rate was one atom every 3 picoseconds (ps). Each timestep an atom was to be inserted; its coordinates were chosen randomly in x and y direction. But the coordinate in z position was set to be at least a user defined distance above the highest current atom in simulation that was “nearby” the chosen x, y position. Here, “nearby” meant the lateral distance (in x, y directions) between the new and existing atoms was less than the interaction cut-off. The deposited atoms were given a velocity in negative z-direction. Velocity in x and y components were zero (i.e. normal deposition vector). The deposited atoms had an average velocity of $0.9 \text{ \AA}/\text{ps}$, corresponding to an average kinetic energy of $8.27 \times$

10^{-3} *ev*. Note that for each simulation, five different random number seeds were used due to the stochastic nature of deposition. In this way, average behaviors can be analyzed, as well as specific behavior in each statistical sample.

Non-frozen atoms in the substrate and island at the start of the simulation are modeled in a NVT ensemble. Deposited atoms are simulated in a NVE ensemble so that deposition trajectories are not altered by the thermostat algorithm. Three normal stress components for each atom and temperature within each group were calculated during simulations. All deposition simulations run for at least 3×10^7 timesteps, which was 30 nanoseconds (*ns*). This corresponds to at least 10,000 atoms deposited. For the simulation cell used, this corresponds to ~ 17 monolayers.

Chapter 4 Results and Discussions

4.1 Initial Coalescence Stress Analysis

Initial coalescence stress is the stress within thin films at the moment when two neighboring islands initially contact each other. Herein, we distinguish initial coalescence stress from on-going coalescence stress. The latter occurs when deposition after initial coalescence create stress. Hoffman initially suggested that tensile stress was generated when two neighboring discrete islands impinge on each other and he proposed a relatively simple model with vertical parallel free surfaces. In such a model, initial coalescence stress was the same as on-going coalescence stress since two parallel free surfaces merged together completely at the moment coalescence happened. However, stress prediction from that model was greater than experimental observation by several orders of magnitude. In this study, a more realistic model with two hemi-cylinder shape free surfaces, as shown in Figure 3-4, was examined. In such model, initial coalescence stress was different from on-going coalescence stress.

Two kinds of models were used, as shown in Figure 3-4 and Figure 3-6, to study the initial coalescence stress. In the model shown in Figure 3-4 two island surfaces contacted each other at the interface between the island and the substrate. Therefore, when MD was first run – in the absence of any deposition – atoms on the island surfaces in x direction were within interaction distance. This caused island atoms in the first few atomic planes closest to the substrate to stretch and merge, as shown in Figure 4-4. So there was initial coalescence stress in this model. In the model shown in Figure 3-6, there was a gap between two neighboring islands so no initial coalescence stress existed in this

model. The initial coalescence stress could be found by comparing the stresses within these two models.

Since coalescence occurred in x-direction, stress in x-direction was examined. LAMMPS produced thermodynamic state information, including 6 independent stress tensor entries, into logfiles. The stress tensor was evaluated as following:

$$\sigma_{IJ} = \frac{\sum_k^N m_k v_{kJ} v_{kI}}{V} + \frac{\sum_k^N r_{kI} f_{kJ}}{V} \quad (22)$$

where I, J are direction indice x, y, z, N is the number of atoms in the system, V is the simulation system volume, m_k is the mass of atom k, v_{kJ} is the velocity of atom k in J direction, r_{kI} is the I direction component of the coordinate of atom k and f_{kJ} is the force on the k atom in the J direction.

Note that LAMMPS calculated stress tensor using total system volume. However, initial coalescence stress was the tensile stress within islands. A correction on volume was needed as following:

$$\sigma'_{xx} = \sigma_{xx} \times \frac{V}{V_{island}} \quad (23)$$

where σ'_{xx} was the average normal stress in x-direction after correction, σ_{xx} was the average normal stress in x-direction, V_{island} was the volume occupied by island atoms. Having the results from two different models, as shown in Figure 3-4 and Figure 3-6, initial coalescence stress could be calculated as

$$\sigma_{initial} = |\Delta\sigma'_{xx}| \quad (24)$$

where σ_{initial} was initial coalescence stress, and $|\Delta\sigma'_{xx}|$ was the difference between average tensile stresses from the two models. Note that finite tensile stress existed for the system with no initial coalescence of islands. This is due to system stress effects on the island free surfaces.

	Substrate Thickness = 5 nm	Substrate Thickness = 10 nm	Substrate Thickness = 20 nm
Average Tensile Stress in Model 1(MPa)	785.0184	1480.244	1301.707
Average Tensile Stress in Model 2(MPa)	511.5776	1036.813	934.5604
Initial Coalescence Stress (MPa)	273.4406	443.4308	367.1466

Table 4 Initial coalescence stress

Table 4 lists the initial coalescence stress results in three simulation systems with different substrate thickness. It is clear for the two larger substrate thickness systems ($H_s = 10$ and 20 nm), average tensile stress σ'_{xx} in the initial coalescence produced relatively similar values around 1400 MPa. However the average tensile stress σ'_{xx} had a significant lower value in the 5 nm substrate thickness system ($H_s = 5$ nm). Model 2 in Table 5 was for the no initial coalescence stress case (i.e. larger gap between islands prevent free surface interaction). Nonetheless, stress exists due to surface effect. Here again, note the value for stress in this case is roughly half the value for $H_s = 5$ nm system, compared to the larger systems ($H_s = 10$ and 20 nm). This is investigated further below but evidence exists, that a 5 nm substrate thickness is too thin so that stress magnitudes are affected by simulation size.

As presented above, two kinds of model shown in Figure 3-4 and Figure 3-6, were used to study initial coalescence stress; in each case, three substrate thicknesses were

studied. To understand the difference between stress behavior for the thinnest substrate system ($H_s = 5$ nm) and the two thicker substrate systems ($H_s = 10$ and 20 nm), we investigated individual, atomic scale contributions to the overall system stress. After computing each atom's contribution to system stress, data were plotted in histogram style as shown in Figures 4-1 to 4-3.

In the histogram stress analysis, atoms in the frozen zone for each system were extracted from the analysis. This is because atoms in the frozen zone were kept static and forces between them were set zero manually. It is clear from histograms that atoms with largest tensile stress are in the magnitude of tens of gigapascals, which are quite high compared to experiment observed values. This is because the individual, atomic stress values shown here were normalized with atomic volume. It is doubtful if stress so defined has the same meaning as continuum scale stress. Nonetheless, this permits us to quantitatively compare individual atomic contributions to the overall system stress.

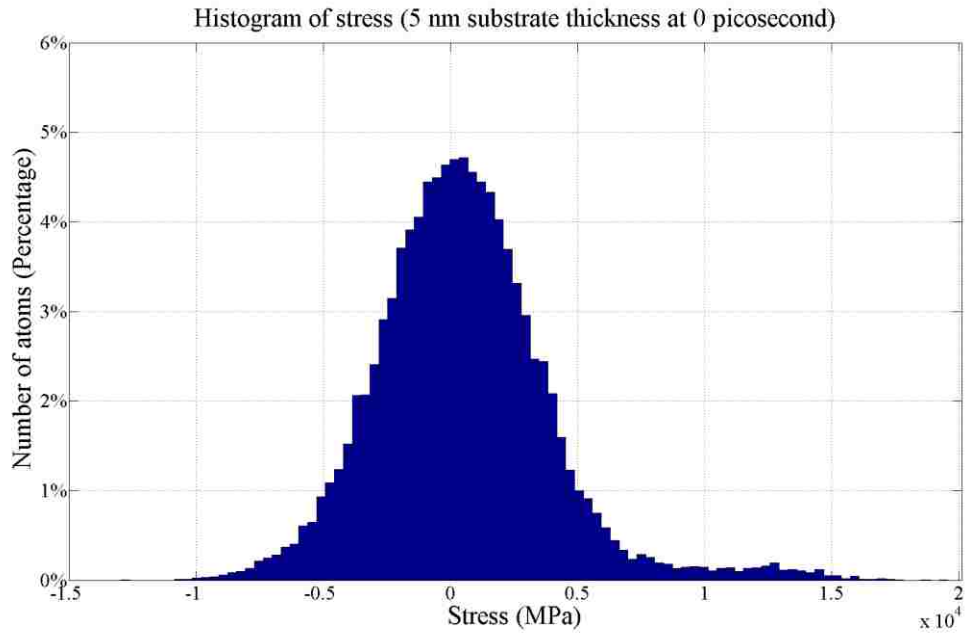


Figure 4-1(a) Histogram of stress for 5 nm substrate system at 0 picosecond

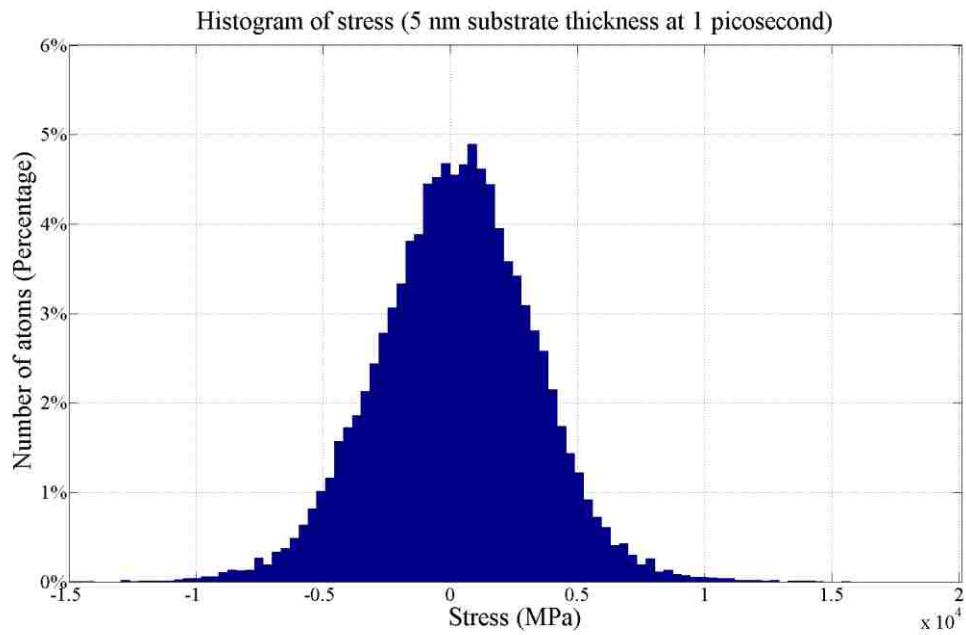


Figure 4-1(b) Histogram of stress for 5 nm substrate system at 1 picosecond

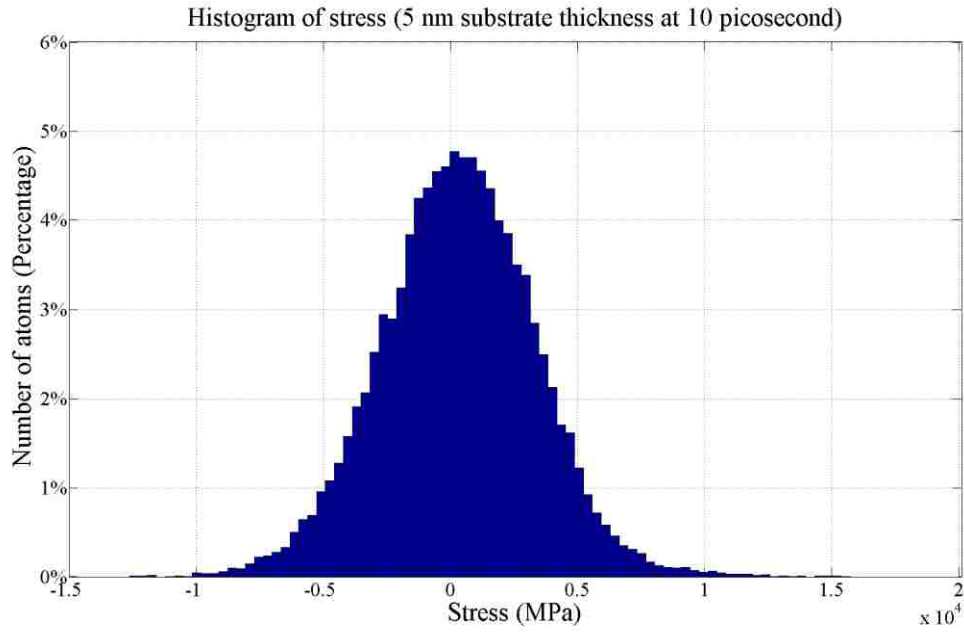


Figure 4-1(c) Histogram of stress for 5 nm substrate system at 10 picoseconds

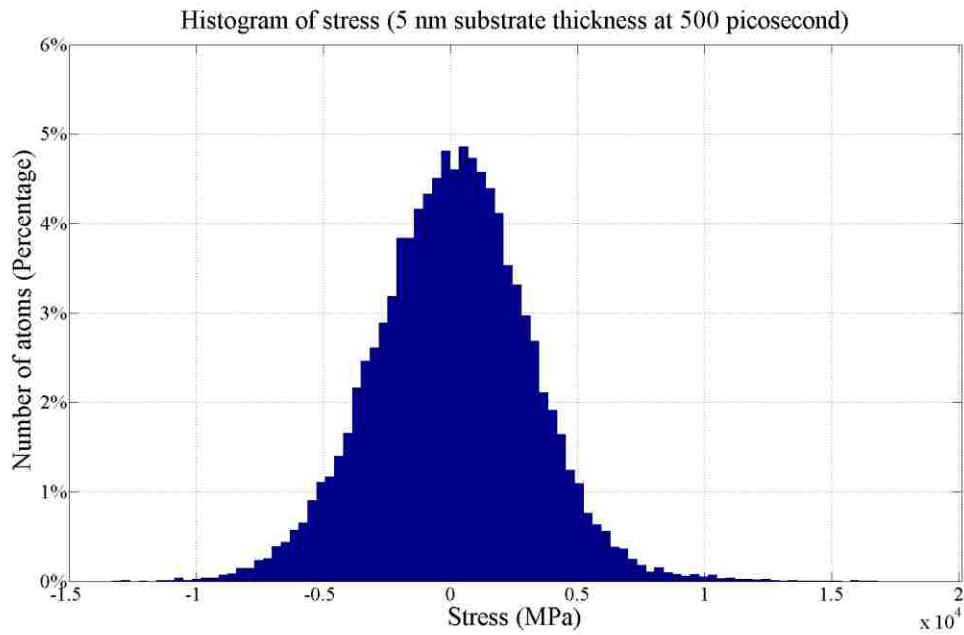


Figure 4-1(d) Histogram of stress for 5 nm substrate system at 500 picoseconds

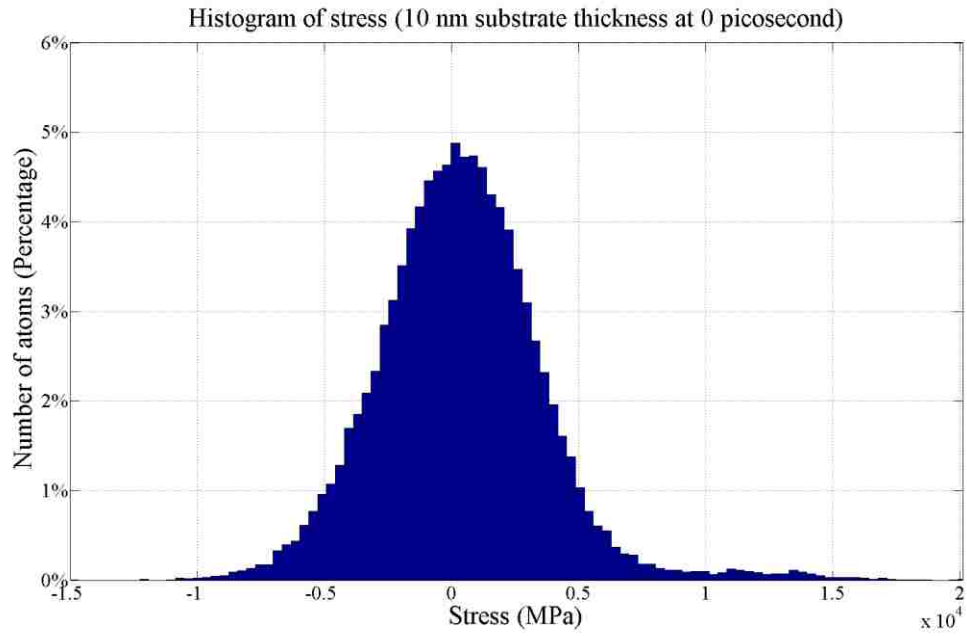


Figure 4-2(a) Histogram of stress for 10 nm substrate system at 0 picosecond

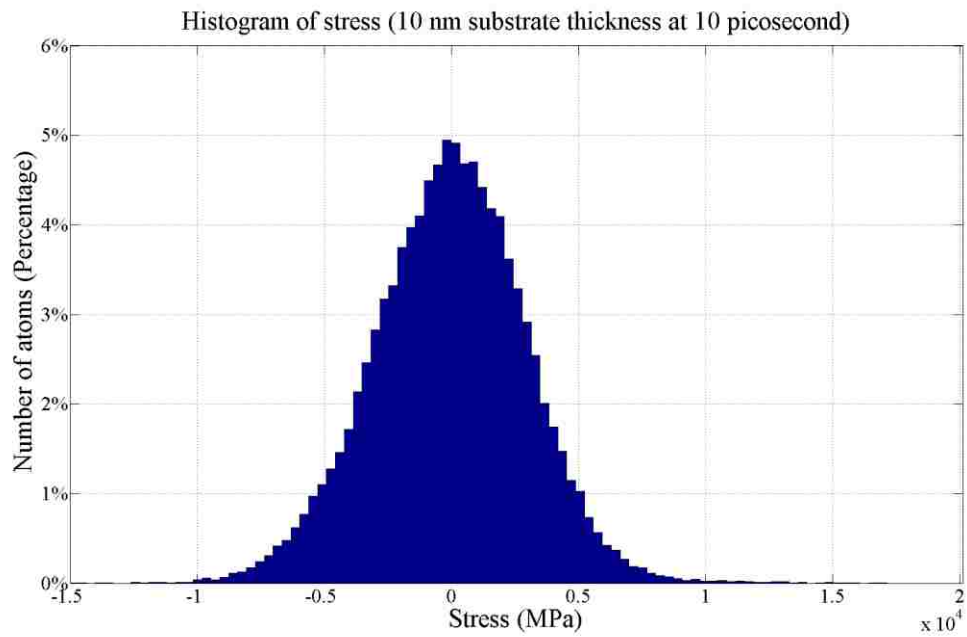


Figure 4-2(b) Histogram of stress for 10 nm substrate system at 10 picoseconds

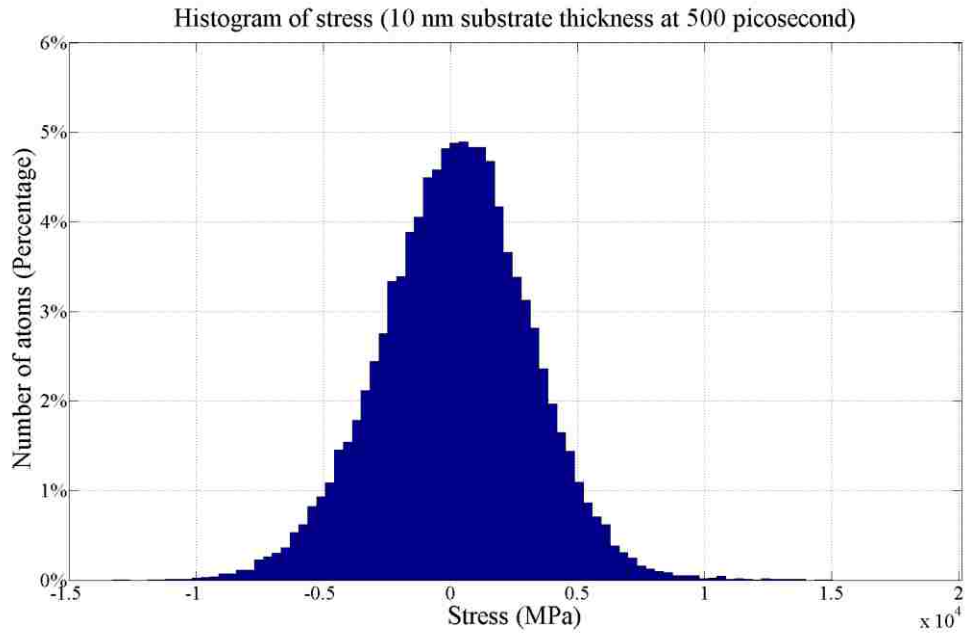


Figure 4-2(c) Histogram of stress for 10 nm substrate system at 500 picoseconds

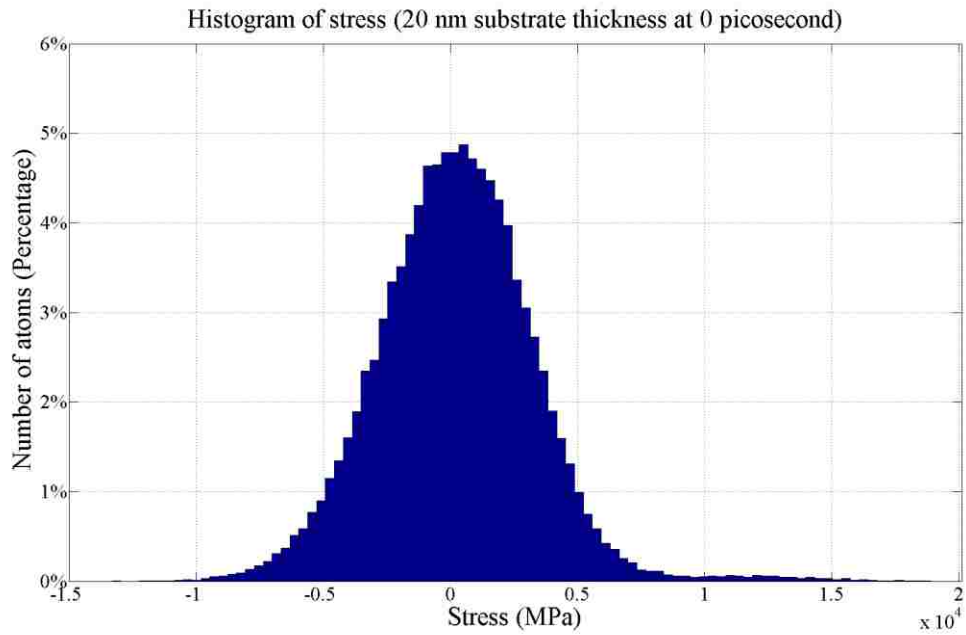


Figure 4-3(a) Histogram of stress for 20 nm substrate system at 0 picosecond

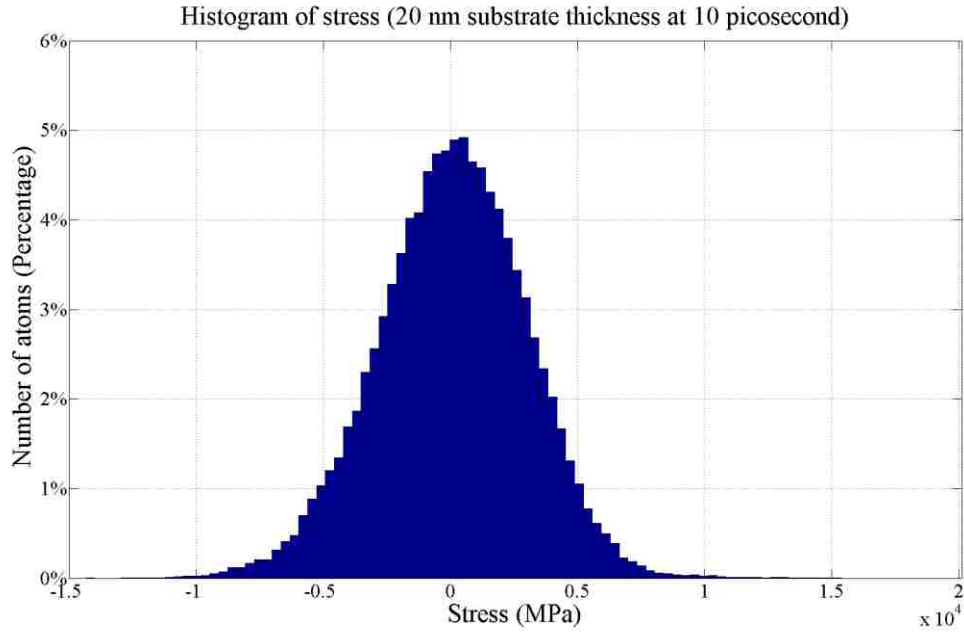


Figure 4-3(b) Histogram of stress for 20 nm substrate system at 10 picoseconds

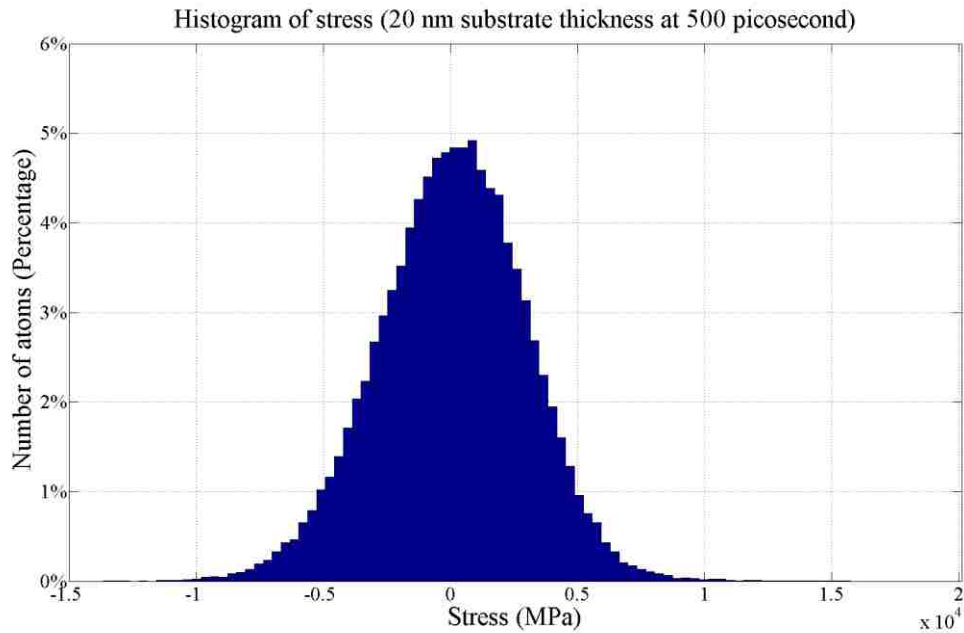


Figure 4-3(c) Histogram of stress for 20 nm substrate system at 500 picoseconds

Consider first Figure 4-1 for the 5 nm substrate thickness system ($H_s = 5$ nm). Data are shown for four times during the simulation $t = 0, 1, 10,$ and 500 ps. It is clear for

all points in time shown that the majority of atoms were in a stress state distributed narrowly around zero, which meant that majority of atoms were in an equilibrium stress state, perturbed only by thermal fluctuations. Attention should be paid to the positive (tensile) stress tail of the histogram at $t = 0$. It is clear that the atoms stress distribution at $t = 0$ have a bigger tail in positive stress range (from $+10^4$ to $+1.5 \times 10^4$ MPa); Figures 4-2(a) and 4-3(a) show the same is true for the thicker substrate systems. The bigger tail at the very beginning of initial coalescence run meant that more atoms in the system contributed tensile stress to the system total. Atoms contributing to this tail were physically located at the free surface of the “as cut” hemi-cylinder island; this was true for all substrate thickness systems. Figure 4-4(a) shows the stress distribution within 10 nm substrate system ($H_s = 10$ nm) at $t = 0$. It is clear that atoms on the hemi-cylinder surfaces exhibited significant tensile stress. Such tensile stress resulted from surface stress due to sudden change in atomistic structure. Those atoms on the hemi-cylinder surfaces lost some of their neighbors after cutting out islands. Such sudden change in atomistic structure induced positive surface stress on those surface atoms, leading them to be in tensile stress state. Figure 4-1(b) shown the per atom stress distribution for the 5 nm substrate thickness system ($H_s = 5$ nm) at $t = 1$ ps. Note that a significant portion of contributions between $+10^4$ to $+1.5 \times 10^4$ MPa are gone after 1 ps of simulation time; nearly every contribution greater than $+1.5 \times 10^4$ MPa is also gone. Figures 4-1(c) and 4-1(d) show 5 nm substrate thickness per atom stress distributions at $t = 10$ ps and 500 ps. These are both quite similar to the $t = 1$ ps result, indicating the majority of relaxation occur very rapidly, even on MD scales. A notable result is that, for $t = 500$ ps, additional tensile stress contributions emerge with magnitude greater than $+1.5 \times 10^4$ MPa; in other

words, while most stress evolution from initial coalescence occurs in the first few ps of simulation time, some relatively long time behavior is also observed. Figures 4-2 and 4-3 show these same observations can be made for the thicker substrate systems. The very rapid stress relaxation in the first few ps of simulation is a result of surface relaxation. Figure 4-4(b) shows the stress distribution within the 10 nm substrate system ($H_s = 10$ nm) at $t = 500$ ps of initial coalescence run. It is clear from Figure 4-4 that atoms on hemicylinder surfaces at $t = 500$ ps exhibited much smaller tensile stress compared to $t = 0$.

As described above, stress magnitudes for the 5 nm substrate thickness system ($H_s = 5$ nm) were consistently lower than those computed for the 10 nm and 20 nm substrate thickness systems ($H_s = 10, 20$ nm), which gave results quite similar to one another. Indeed, one can consider the stress in each system at $t = 0$, before any relaxation has occurred. Note that there is no difference in the three substrate thickness systems at this point (except for the substrate thickness). Put differently, in all three systems, islands have just been extracted and no relaxation has occurred so island atoms in all three systems occupy equivalent positions. Nonetheless, even at this point in the analysis, the 5 nm thickness substrate system ($H_s = 5$ nm) has σ'_{xx} that is 33% lower than the values computed for both of the thicker substrate systems. Further note the two thicker substrate systems, at $t = 0$, have tensile stress magnitudes that differ from one another by 1%. What this means is that, even in the absence of island relaxation, the smallest thickness substrate system introduces a simulation artifact in that stress magnitudes are artificially depressed. Considering the expression for stress in Equation (22), the difference observed for 5 nm substrate thickness system ($H_s = 5$ nm) must result from differences in the second term on the right hand side of the expression. This is because

all three thickness systems are $T = 300$ K so the kinetic energy term is equal in all cases. The implication is that positive contributions that are present for the thicker substrate systems are not for the $H_s = 5$ nm system. The further implication is that the missing contributions come from substrate atoms that are greater than 5 nm from the island/substrate interface. Since both thicker substrate systems give very similar results for stress magnitudes, it was concluded that - for this island size - $H_s = 10$ nm was sufficient to conduct ongoing coalescence simulations. What remains unknown is the direct relationship between the island size simulated and the corresponding minimum H_s . Here, substrate thickness equal to the island radius introduced simulation artifacts whereas thickness two times the radius was sufficient to avoid them. Future work will examine this relationship in greater depth since it is important to know the minimum computational resources required to obtain reliable simulation results. Using too large a substrate thickness is more computationally costly and should be avoided if possible. For the remainder of this thesis substrate thickness of 10 nm was used.

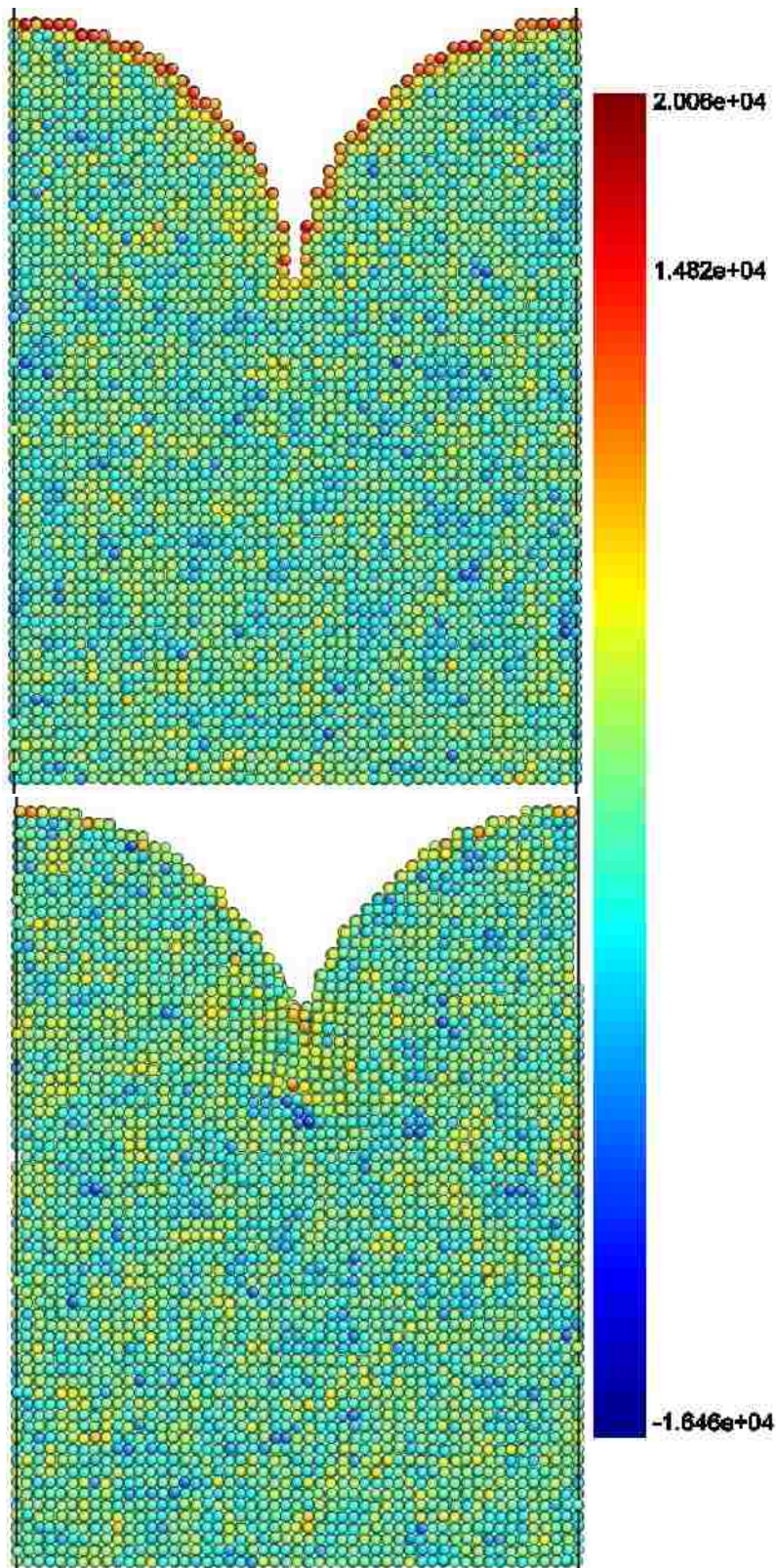


Figure 4-4(a) Stress distribution coloring for 10 nm substrate system at 0 ps of initial coalescence run. The color bar shows stress in MPa.

Figure 4-4(b) Stress distribution coloring for 10 nm substrate system at 500 ps of initial coalescence run

4.2 Intrinsic Stress Evolution Behavior

In Volmer-Weber growth for high mobility atomic species, intrinsic stress evolution exhibits a compressive-tensile-compressive behavior: compressive stress is observed in pre-coalescence films, tensile stress is observed during island coalescence and grain growth, and compressive stress develops again after island coalescence as the continuous film thickens. The fundamental property of interest in this study was the intrinsic tensile stress evolution during on-going coalescence in high-mobility Volmer-Weber growth mode. Having results from five thermodynamically equivalent but statistically distinct deposition simulations, intrinsic stress as a function of effective film thickness, and force per unit width against effective film thickness, are plotted in Figure 4-5 and Figure 4-6, respectively. The effective thickness of islands can be determined by

$$h_{effective} = \frac{N_{islands}}{N_{monolayer}} \times 2.05\text{\AA} \quad (25)$$

where $h_{effective}$ is the effective thickness of islands. $N_{islands}$ and $N_{monolayer}$ are number of atoms in islands and number of atoms in one ideal crystalline monolayer, respectively. To decrease statistical fluctuations intrinsic stress data were time-averaged by taking an average of every one hundred consecutive values. The first few stress values were smoothed as follow:

$$\begin{aligned} YY(1) &= Y(1) \\ YY(2) &= (Y(1) + Y(2))/2 \\ YY(3) &= (Y(1) + Y(2) + Y(3))/3 \\ &\dots \dots \end{aligned} \quad (26)$$

where $Y(i)$ was the original stress value and $YY(i)$ was the smoothed value.

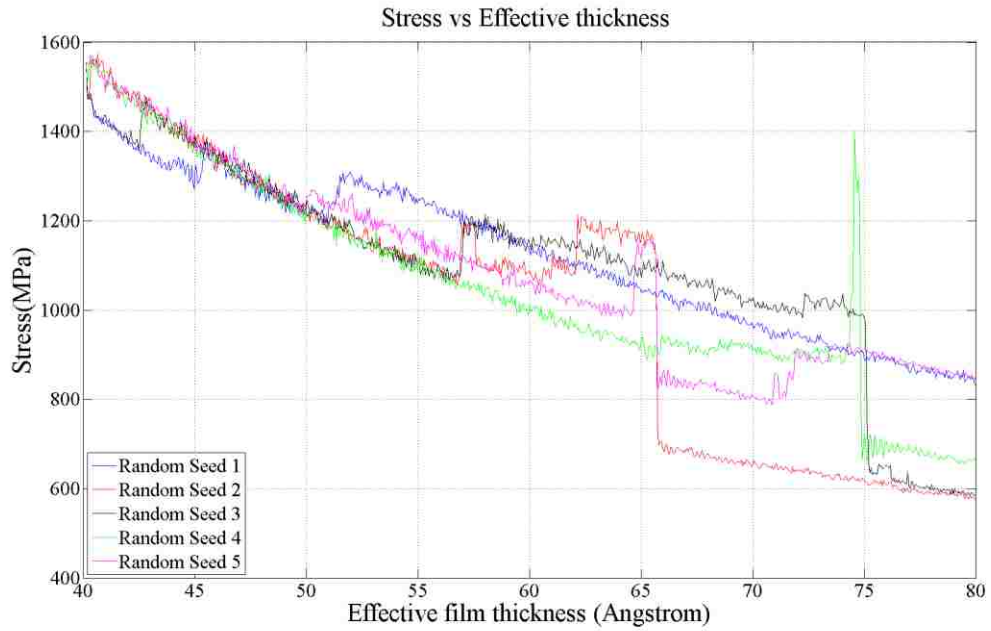


Figure 4-5 Intrinsic stress against effective film thickness

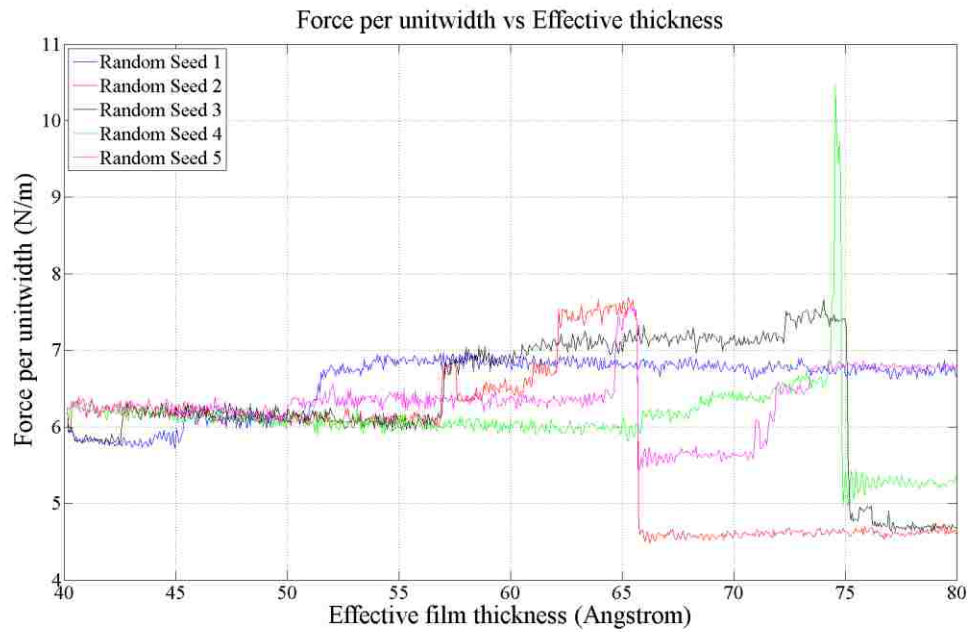


Figure 4-6 Force per unit width against effective film thickness

It was clear from Figure 4-5 that intrinsic tensile stresses in all deposition simulations started at around 1480 MPa at the very beginning of the simulations. Note that tensile stress here was overall system stress, including coalescences stress and surface stress. Because we are interested in understanding how both coalescence and surface stress effects evolve, we studied the overall system stress behavior. As deposited atoms arrived at the island free surface and the film grew, intrinsic tensile stresses had an overall trend of *compressive* evolution. However several sudden jumps up in tensile stress occurred in each simulation and sudden jumps down in tensile stress were observed in all simulations except for random seed 1. The overall trend of decreasing in tensile stress may result from removal of island curvature. This could be understood from the pressure and surface stress relationship:

$$\sigma = -P = -\frac{2f}{r} \quad (27)$$

where σ is stress, P is pressure, f is surface stress, and $1/r$ is radii of curvature of islands. Because we model an ideal system where the islands and the substrate material are identical, this means that, when the islands are formed, they are ideally bound to the substrate. The island has very small radius, indicating significant compressive stress would manifest in an unconstrained island. An unconstrained island would, of course, be in mechanical equilibrium: compressive internal stress would balance tensile surface stress. However, because the island atoms near the substrate are highly constrained to remain at bulk equilibrium lattice spacing, they do not contact as much as they would in an unconstrained case. This manifests tension in the islands, even in the absence of coalescence. As the island grows and the hemicylindrical surface approaches a flat

surface, pressure due to effects represented by equation 27 becomes less. As such, those atoms that were initially at the island/substrate interface are at the proper lattice spacing such that a source of tensile stress contribution is removed. This would manifest as a compressive evolution. However, there is another effect.

The pressure that is induced inside a small solid body due to surface stress can be thought of as a compression that balances tension in an elastic skin on the body. The elastic skin is the free surface. Thus, the effect is one whose magnitude is related to the surface to volume ratio of a given system. One can consider a system where atoms are carefully deposited onto the hemicylindrical islands such that the gap is perfectly filled in and the final state is a uniform, flat crystal surface with corresponding film thickness equal to the initial island radius. If one considers the surface area to volume ratio of this ideal film, it is $S/V = 1/r$, where r is the initial island radius. For the initial island, however, $S/V = 2/r$. As such, surface to volume effects for the hemicylindrical thin film are of order two times what they are for a flat film of the corresponding thickness. Thus, simply going from an array of hemicylindrical islands to a flat surface will remove the percentage of atoms that are in surface states, compared to bulk crystal states and this too will generate significant reduction in tensile stress contributions. Again, this manifests as compressive evolution.

The stress-effective film thickness product ($\sigma h_{effective}$) was plotted versus effective film thickness in Figure 4-6. Thus, the derivative of $\sigma h_{effective}$ with respect to $h_{effective}$ gives the instantaneous stress in the film, i.e. the stress in the currently deposition layer. On the other hand, the total $\sigma h_{effective}$ divided by total $h_{effective}$ gives

the volume average stress in the film. It is clear that $\sigma h_{effective} = 6.2 \text{ N/m}$ at the very beginning for all 5 simulations. Then the stress-thickness product increased by several jumps up before the effective film thickness reached 6.5 nm. After that several drops in stress-thickness product were observed in all simulations except for random seed 1. At the end of simulations, stress-thickness product of random seed 1 and 5 converged at around 6.8 N/m and stress-thickness product of the other three simulations converged at around 4.9 N/m. Note that volume average stress for random seed 1 and 5 simulations is in the magnitude of 1.5 GPa, which is relatively higher than experimental values. The relative high stress can be caused by the following two reasons: our system is an infinite array of hemicylindrical islands that all behave in a time simultaneous fashion. Furthermore, we are studying island size of 5 nm radius; all contributions to stress evolution are expected to be at a maximum for the smallest island sizes. As a result, our systems present upper limits to stress evolution behavior.

We utilize five random number seeds to start five statistically independent but thermodynamically equivalent simulations in the hopes of obtaining some average, convergent data. However, results presented demonstrate that two of the systems show net tensile evolution and three show net compressive evolution; furthermore, the magnitudes of volume average stress over the 4 nm of additional material deposited are large in all cases (i.e. large compression and large tension). Above, the large stress magnitudes were addressed. However, lack of consistency among the five simulations is of greater concern and it is this lack of consistency among our data sets that points to some of the shortcomings in our methodology. Most specifically, simulations have not been run long enough. As can be seen in Figures 4-9 (a - e), none of the systems have

reached a relatively flat film by the end of the simulations. In some cases, the presence of the initial gap between islands is still fairly obvious. In other systems, the gap closes in some spots, but the growing free surface still possesses significant surface roughness. These observations indicate that the regime associated with coalescence is not complete in our simulations and that they need to be run further in time. Future work will investigate this.

Another shortcoming of our methodology is the temporal constraints on molecular dynamics simulations. The effective deposition rate utilized herein is 1 atom every 3 ps; converted to macroscale units (by accounting for our simulation cell dimensions), this is 0.4 m/s, which is equivalent to depositing Mt. Everest in one day. Comparing to typical deposition rates in Table 2, this is at least seven orders of magnitude larger than what is used in experiment. Since stress evolution behavior is known to depend upon deposition flux, discussion of our results must take this vast discrepancy into account. Put simply, this means that atoms do not have anywhere near as much time in our simulations to sample surface sites as they do in experiment. Essentially, atoms stick where they first land. Depending on this, for the results presented here, either removal of surface curvature and area or gap coalescence events dominate, giving either net compressive or tensile evolution, respectively. To understand whether a single convergent behavior exists for this limit of very high deposition rate, longer simulations are required. Indeed, despite the temporal constraints on MD deposition rates, it would still be interesting to repeat these simulations with flux at the lowest rate that might be studied in a reasonable time. At least one order of

magnitude slower is possible, perhaps two, but these require simulations to run for months of wall clock time.

Despite the conclusion above that longer time scale must be accessed to fully elucidate phenomena of on-going coalescence, current results still permit us to examine atomistic mechanism associated with discontinuous stress-thickness ($\sigma h_{effective}$) changes. First, we must explain their presence since they are typically not observed in experiments. The primary reason for the occurrence of such discontinuous $\sigma h_{effective}$ changes is our simulation setup: though only one explicit island is modeled, periodic boundary condition in x direction makes this a model of an infinite array of uniform islands in x direction. Once some atomistic structure change happens that causes intrinsic stress change in one island, it is as if it happened to every island on a substrate surface at precisely the same time. So a large, discontinuous change in $\sigma h_{effective}$ happens. In an experiment, different islands would exhibit coalescence at different time, giving more gradual changes in σh .

In the following, descriptions and explanations of some discontinuous stress evolution mechanism in our simulations of V-W growth mode are given, using random seed 1 and random seed 2 simulations as examples. Note these are cases where one (random seed 1) showed net tensile stress evolution whereas another (random seed 2) showed net compressive evolution.

In Random Seed 1 simulation, it was clear that there were two significant jumps up in tensile stress evolution. The first jump occurred near 5×10^6 timesteps (film thickness ≈ 4.5 nm) and led to around 100 MPa rise in tensile stress due to the cohesive

force between two neighboring islands. The deposition process continuously added material to the growing surface; a significant portion of depositing atoms entered the space between two neighboring islands. Such process resulted in structural changes for atoms in the gap. Figure 4-7(a) and 4-7(b) showed the configuration snapshot before and after the first jump, respectively. It is clear that atoms in the cusp became more ordered after the jump, whereas they were relatively disordered before (see circled region in Figures). The jump in tensile stress may be caused by the elimination of defects in the cusp that caused compressive stress. The second jump up in tensile stress occurred near 1×10^7 timestep (film thickness ≈ 5.1 nm) due to coalescence of two neighboring islands. It was clear from Figure 4-7 (c) and (d) that as atoms deposited into the gap, two neighboring island surfaces grew sufficiently close to each other that a small group of atoms adopt strained positions so as to close the gap, resulting in the formation of grain boundary and an increase in tensile stress. In this case, we concluded the free surface energy reduction is greater than elastic energy increase so that the formation of grain boundary occurred.

In Random Seed 2 simulation, there were two relatively large jumps in tensile stress: one of magnitude of ~ 120 MPa near 1.5×10^7 timestep (film thickness ≈ 5.7 nm) and another of magnitude ~ 100 MPa near 2.0×10^7 timestep (film thickness ≈ 6.2 nm). Part of the tensile stress generated from the first event was relieved fairly quickly after the first event; however, it then reemerged with the second event. Figure 4-8(a), (b) and Figure 4-8(c), (d) showed simulation snapshots before and after the first and second events, respectively. Consider Figure 4-8(a) before the first tensile stress increase, there was a clearly gap between two neighboring islands, whereas Figure 4-8(b) showed that

two islands contacted each other in the middle of the gap. A small part of grain boundary was formed, resulting in tensile stress increase. Similar phenomenon was observed during second tensile stress increase: more parts of islands contacted each other and the grain boundary grew further.

However, for Random Seed 2 simulation, there was a drop back in tensile stress after two jumps up, which was not observed in Random Seed 1 simulation. The drop back in tensile stress occurred near 2.25×10^7 timestep (film thickness ≈ 6.6 nm), leading to a drop of ~ 450 MPa in tensile stress. At the same time, a great change in atomistic structure of the system was observed: a defect in the substrate and a defect in the island vanished together. The elimination of those two defects was facilitated by the proximity of the free surfaces; in this case, those defects were the sources of tensile stress and their elimination led to the decrease in tensile stress, shown in Figure 4-8 (e) and (f).

Note that the elimination of defect in Random Seed 1 simulation resulted in tensile stress increase (i.e. that system's first positive jump), whereas that in Random Seed 2 simulation led to huge relief of tensile stress. This is because defect in Random Seed 1 simulation located strictly at the cusp. Atoms in that region before the tensile jump were in a compressive state because atoms were minimizing free surface energy by forcing their way into effectively a small grain boundary. This is akin to the grain boundary insertion theory of compressive stress evolution. Upon further addition of material, the local grain boundary annihilates, atoms adapt more regular crystallographic positions, and both surface energy and elastic energy are lowered. The elimination of that defect relieved such compressive stress and led to a tensile stress increase. However, in

Random Seed 2 simulation, one defect was in bulk phase. In this case, we conclude the bulk defected region contributed significant tensile stress. Elimination of the bulk defects dominated the stress response and resulted in tensile stress relief (or compressive evolution).



Figure 4-7 (a) Configuration Snapshot before the first jump near 5×10^6 timestep (Random Seed 1)



**Figure 4-7 (b) Configuration Snapshot after the first jump near 5×10^6 timestep
(Random Seed 1)**



Figure 4-7 (c) Configuration Snapshot before the second jump near 10^7 timestep
(Random Seed 1)

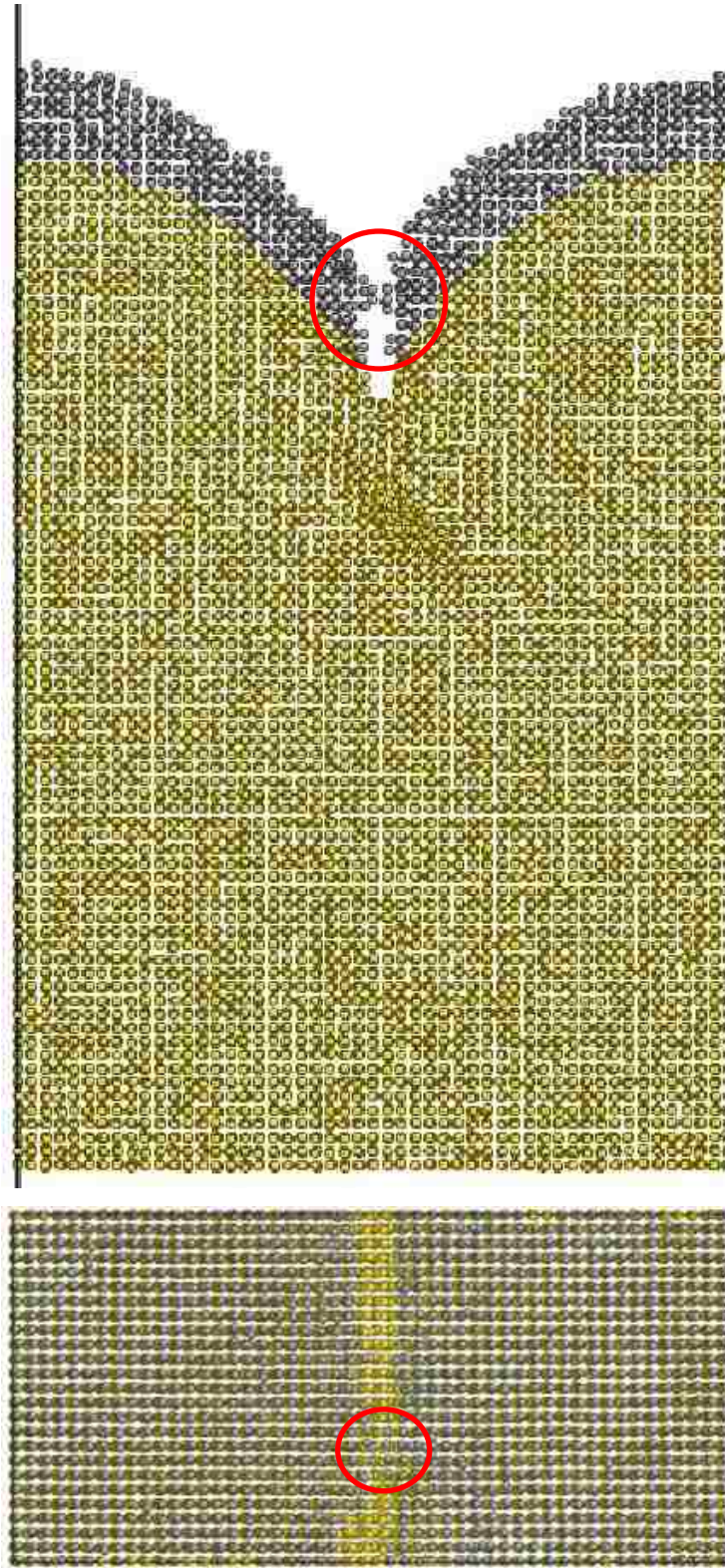


Figure 4-7 (d) Configuration Snapshot after the second jump near 10^7 timestep
(Random Seed 1)

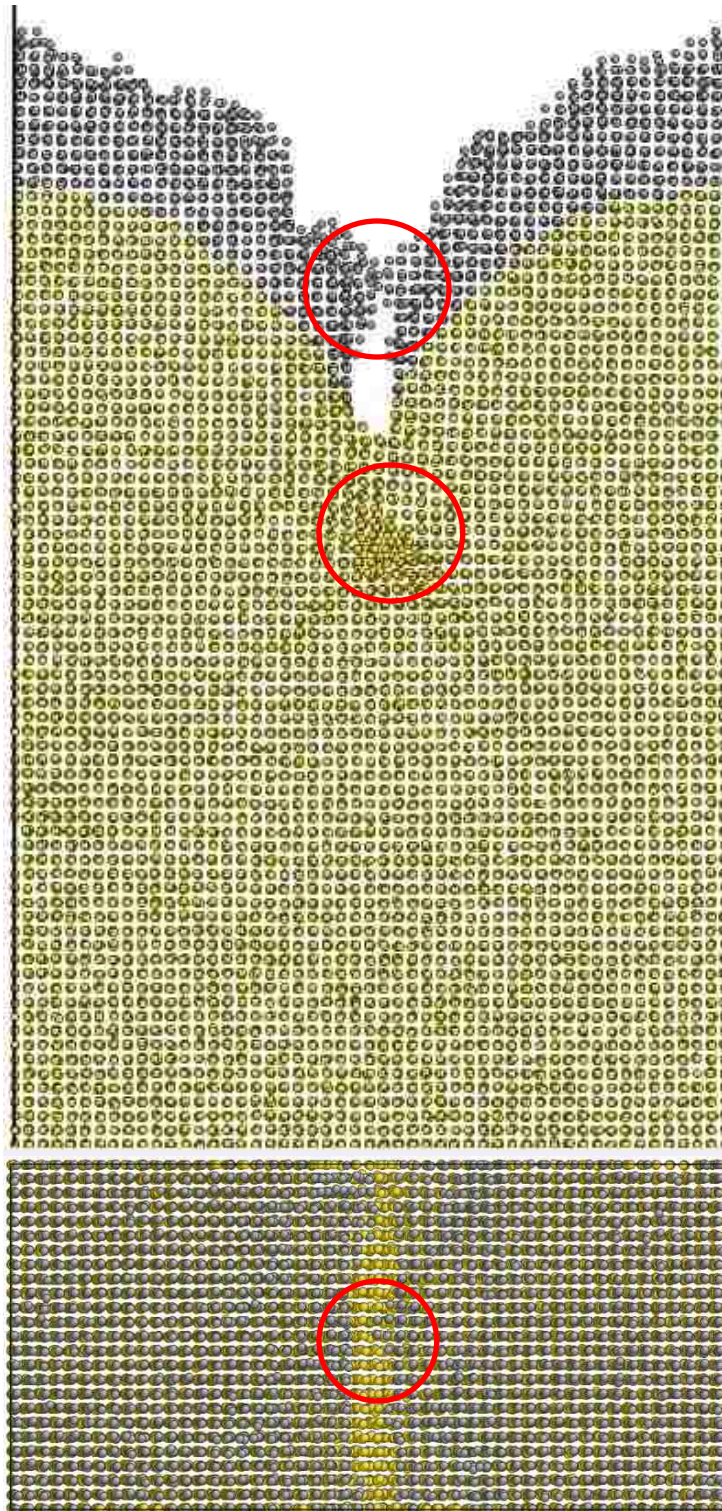


Figure 4-8 (a) Configuration Snapshot before the first jump near 1.5×10^7 timestep (Random Seed 2)

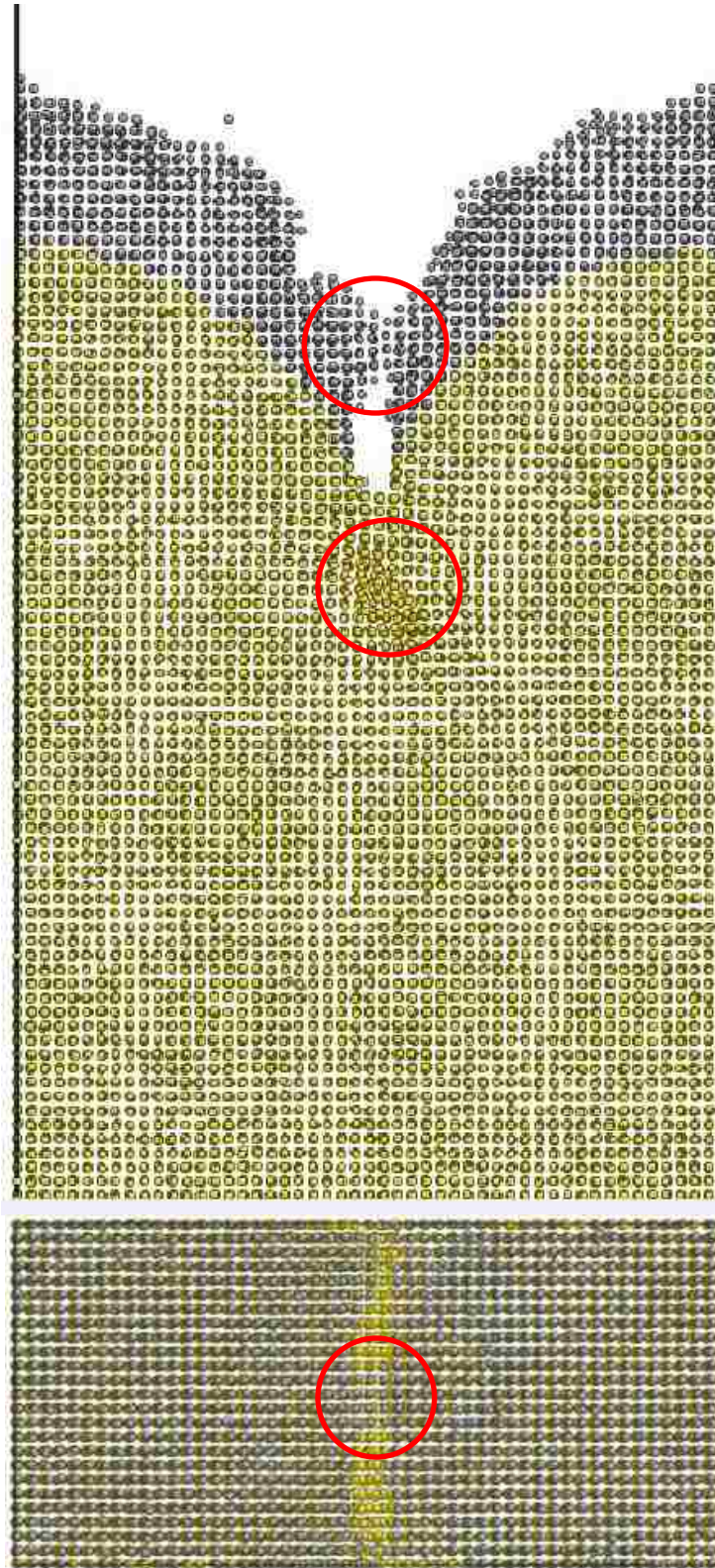


Figure 4-8 (b) Configuration Snapshot after the first jump near 1.5×10^7 timestep (Random Seed 2)

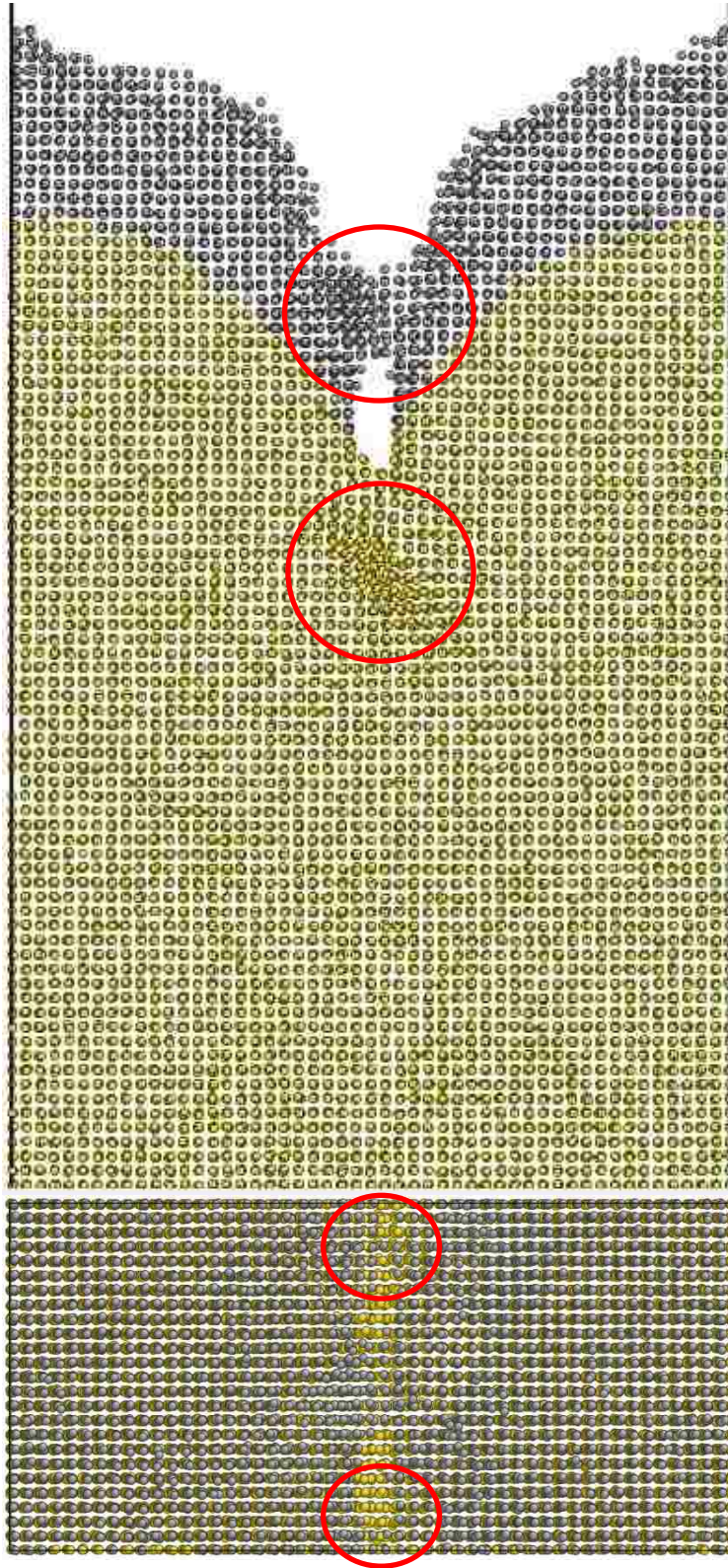


Figure 4-8 (c) Configuration Snapshot before the second jump near 2×10^7 timestep (Random Seed 2)



Figure 4-8 (d) Configuration Snapshot after the second jump near 2×10^7 timestep (Random Seed 2)

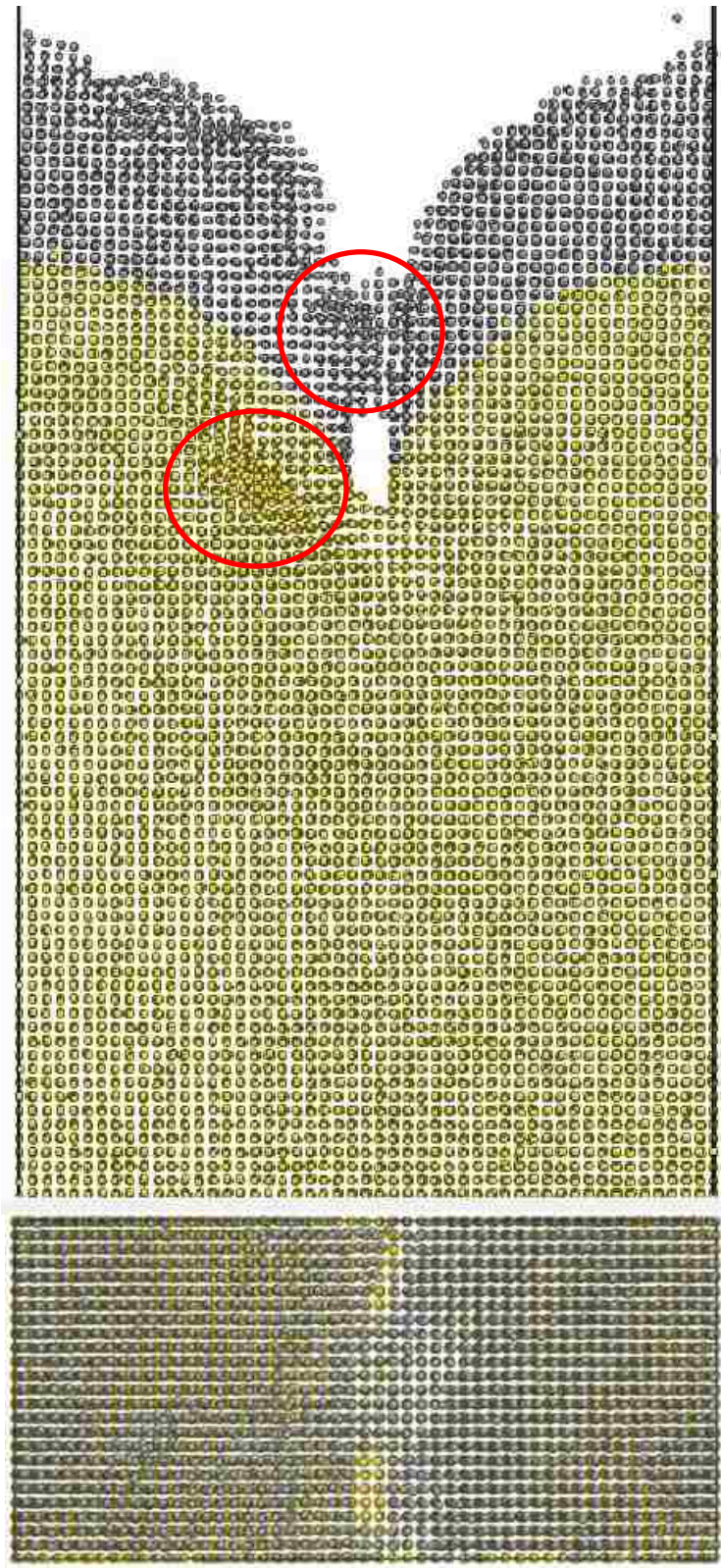


Figure 4-8 (e) Configuration Snapshot before the drop near 2.25×10^7 timestep
(Random Seed 2)

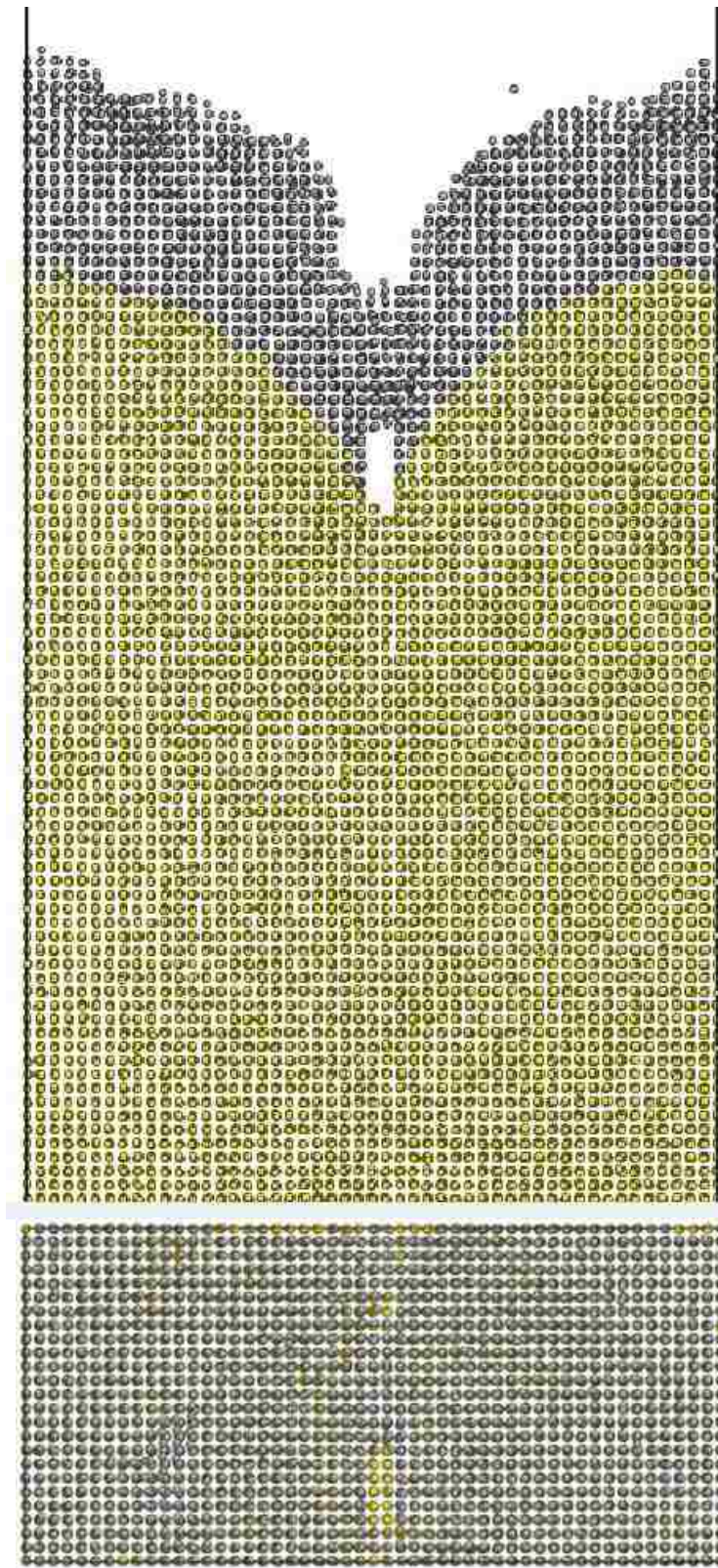


Figure 4-8 (f) Configuration Snapshot after the drop near 2.25×10^7 timestep
(Random Seed 2)

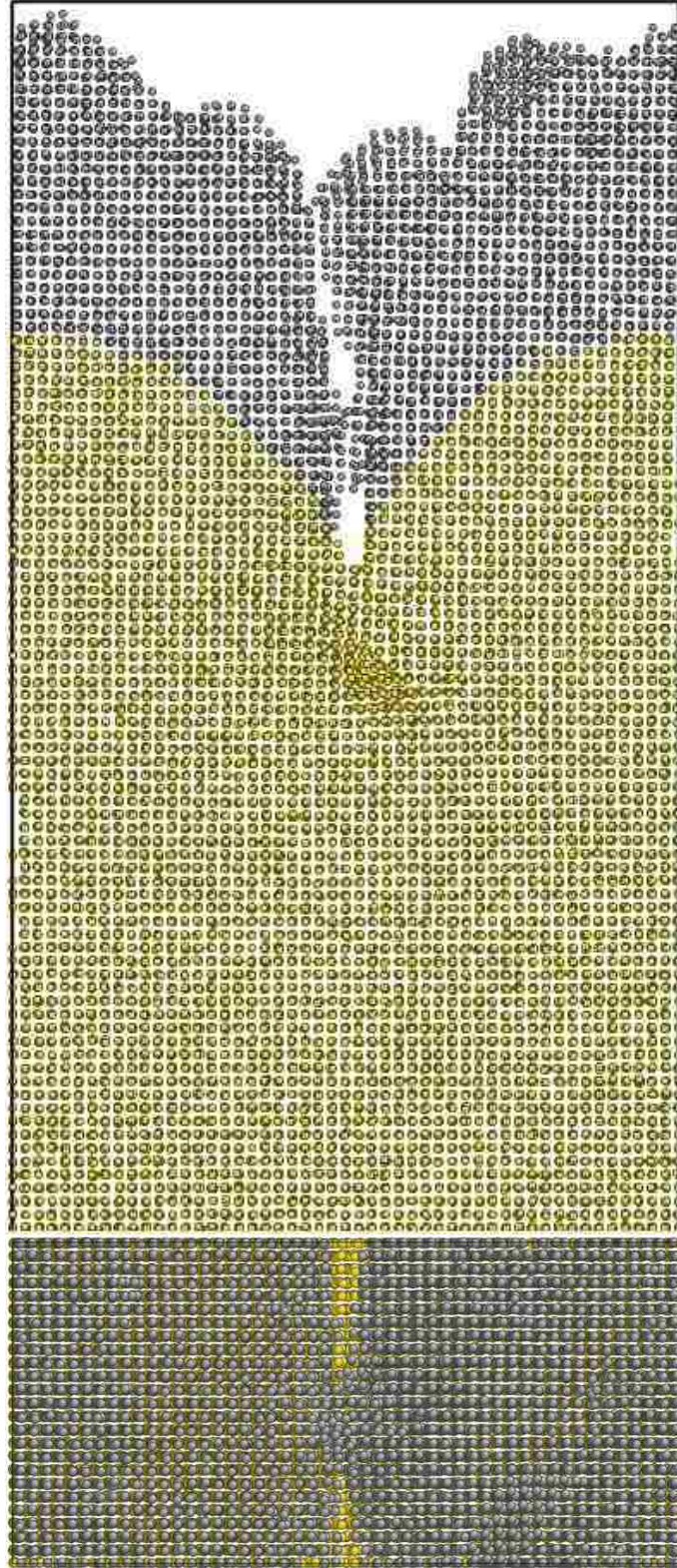


Figure 4-9 (a) Configuration Snapshot at the end of simulation at 3.501×10^7 timestep (Random Seed 1)

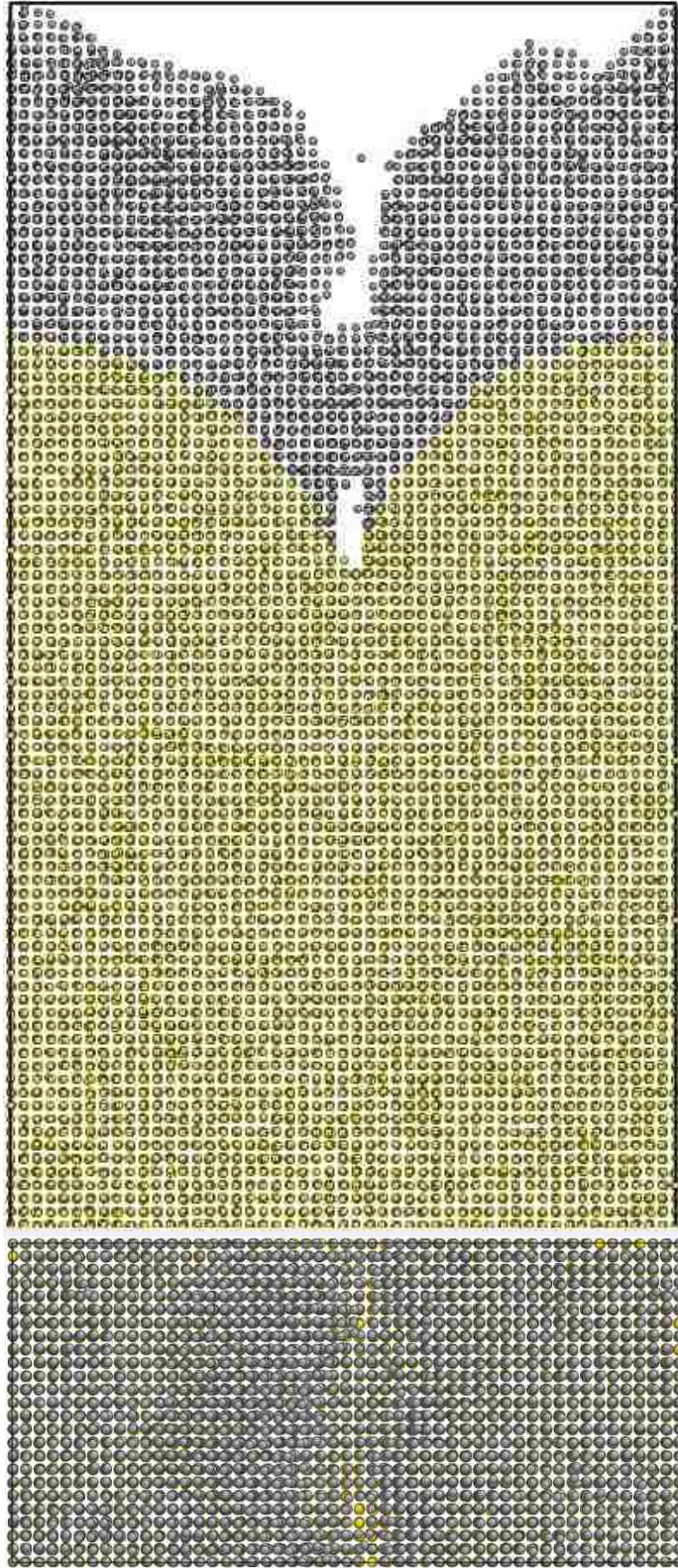


Figure 4-9 (b) Configuration Snapshot at the end of simulation at 3.501×10^7 timestep (Random Seed 2)



Figure 4-9 (c) Configuration Snapshot at the end of simulation at 3.501×10^7 timestep (Random Seed 3)

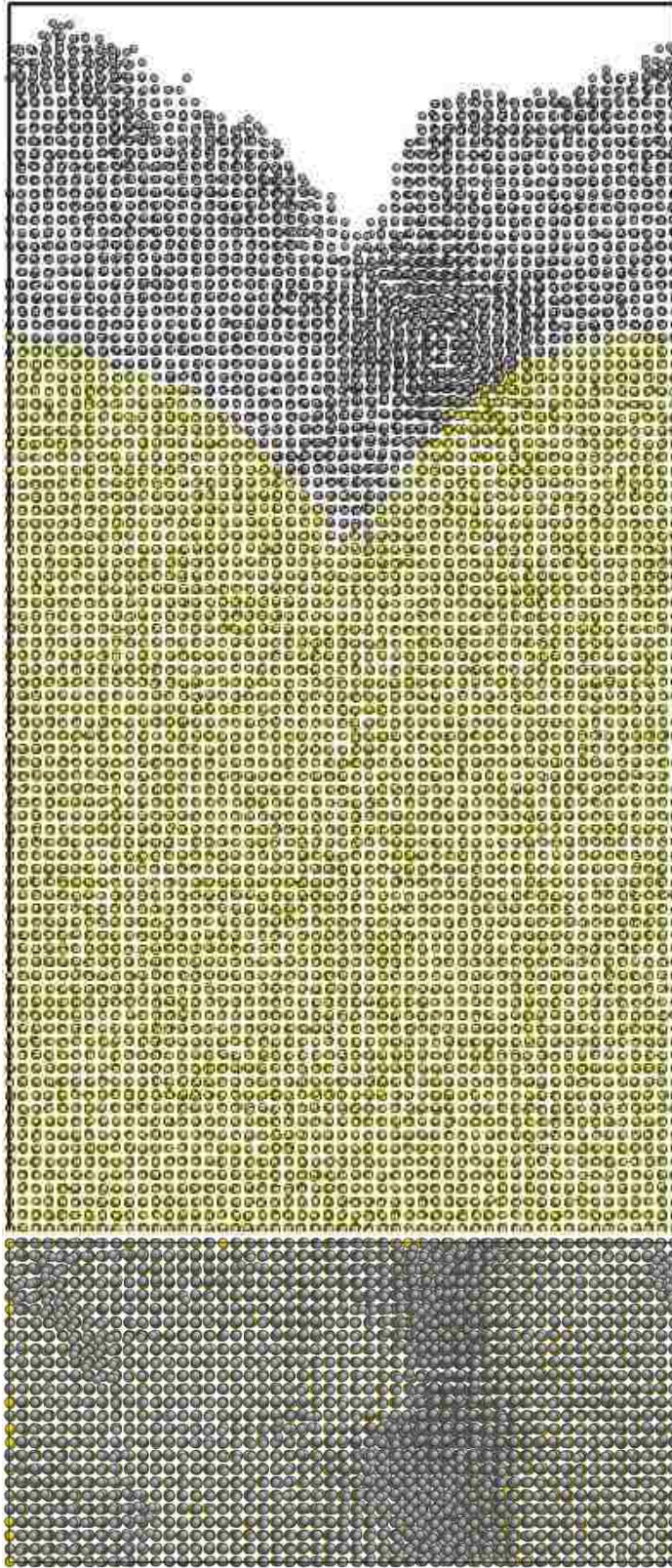


Figure 4-9 (d) Configuration Snapshot at the end of simulation at 3.501×10^7 timestep (Random Seed 4)

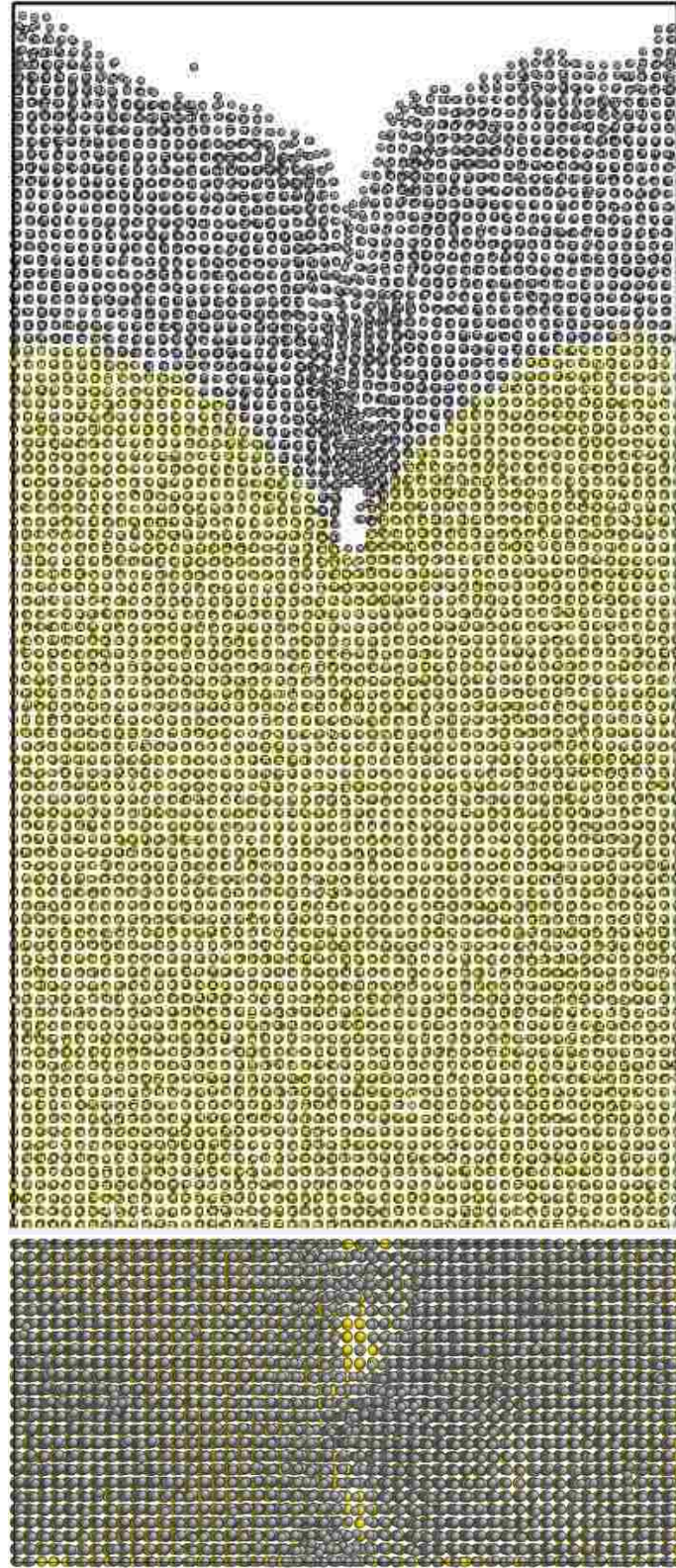


Figure 4-9 (e) Configuration Snapshot at the end of simulation at 3.501×10^7 timestep (Random Seed 5)

Chapter 5 Summary and Future Work

In the previous chapters, tensile stress evolution during Au thin film growth in Volmer-Weber mode was investigated via atomic scale, Molecular Dynamics simulations. Efforts were focused on the on-going coalescence process, which meant that stress evolution was elucidated during the process of free surfaces coalescence and boundary formation.

A model with two hemi-cylinder shape free surfaces was proposed and stress evolution during on-going coalescence process was examined in this study. In on-going coalescence, two neighboring free surfaces merged together as deposited atoms occupied the gap between two free surfaces, resulting in growth of a grain boundary. A nanovoid was sometimes formed in this process.

Stress evolution behavior was elucidated in this model. First, initial coalescence stress was calculated. Then histogram analysis of atomic scale contributions to stress and stress distribution analysis were presented. Furthermore, models with three different substrate thicknesses were examined to determine the appropriate substrate thickness for deposition simulations. It was shown that systems with 10 nm thickness substrates were the best choice for deposition simulation. Given this, intrinsic stress evolution behavior was examined. Stress versus effective film thickness and stress-thickness product versus effective film thickness were plotted for five different random seed simulations. Average behaviors and corresponding mechanisms were presented.

In this study, stress evolution behaviors during coalescence process under certain deposition rate and deposition energy were examined. However, it is interesting to understand stress evolution behavior in general situations. A natural extension of this thesis work should be to investigate stress evolution with different deposition rate, different deposition energy and different size systems.

The effect of deposition rate on intrinsic stress within thin films is not well understood. Del Vecchio and Spaepen[24] used *in situ* stress measurement to analyze the effect of changing the deposition rate on the development of stress in copper and silver thin films. The thickness at which the tensile stress maximum occurred and the average stress in the film at this thickness were measured. The effect of deposition rate on intrinsic stress in gold thin films will be an interesting extension of this thesis work. The deposition rate in this study is very fast compared to thin film deposition in real world. A slow deposition rate would mimic more realistic experiment condition, but also need a longer computational time.

Another extension is to elucidating the influence of deposition energy on intrinsic stress evolution within thin films. D.M. Zhang et al.[25] used kinetic Monte Carlo (MC) method to study the effect of deposition energy on island size. However they did not cover the influence on intrinsic stress. The effect of islands size on intrinsic stress within thin films is also interesting to study. In this study, islands with a diameter of 10 nm were examined. In future simulations, larger size islands can be studied to determine the effect of island size on intrinsic stress behavior within thin films.

Reference

1. Smith, D.L., *Thin-film deposition: principles and practice*. 1995, New York: McGraw-Hill, Inc.
2. Ohring, M., *Materials Science of Thin Films* 2001, New York: Academic Press.
3. Floro, J.A., et al., *Physical origins of intrinsic stresses in Volmer-Weber thin films*. *Mrs Bulletin*, 2002. **27**(1): p. 19-25.
4. Chason, E., et al., *Origin of Compressive Residual Stress in Polycrystalline Thin Films*. *Physical Review Letters*, 2002. **88**(15).
5. Sheldon, B.W., J.D. Nicholas, and S. Mandowara, *Tensile Stress Evolution During the Early-Stage Constrained Sintering of Gadolinium-Doped Ceria Films*. *Journal of the American Ceramic Society*, 2011. **94**(1): p. 110-117.
6. Sheldon, B.W., K.H.A. Lau, and A. Rajamani, *Intrinsic stress, island coalescence, and surface roughness during the growth of polycrystalline films*. *Journal of Applied Physics*, 2001. **90**(10): p. 5097-5103.
7. Markov, I.V., *Crystal Growth for Beginners: Fundamentals of Nucleation, Crystal Growth, and Epitaxy*. 1995, Singapore: World Scientific
8. Cammarata, R.C., *SURFACE AND INTERFACE STRESS EFFECTS IN THIN-FILMS*. *Progress in Surface Science*, 1994. **46**(1): p. 1-38.
9. Cammarata, R.C., T.M. Trimble, and D.J. Srolovitz, *Surface stress model for intrinsic stresses in thin films*. *Journal of Materials Research*, 2000. **15**(11): p. 2468-2474.
10. Hoffman, R.W., *STRESSES IN THIN-FILMS - RELEVANCE OF GRAIN-BOUNDARIES AND IMPURITIES*. *Thin Solid Films*, 1976. **34**(2): p. 185-190.
11. Nix, W.D. and B.M. Clemens, *Crystallite coalescence: A mechanism for intrinsic tensile stresses in thin films*. *Journal of Materials Research*, 1999. **14**(8): p. 3467-3473.
12. Freund, L.B. and E. Chason, *Model for stress generated upon contact of neighboring islands on the surface of a substrate*. *Journal of Applied Physics*, 2001. **89**(9): p. 4866-4873.

13. Nix, W.D., *MECHANICAL-PROPERTIES OF THIN-FILMS*. Metallurgical Transactions a-Physical Metallurgy and Materials Science, 1989. **20**(11): p. 2217-2245.
14. Abermann, R. and R. Koch, *INSITU STUDY OF THIN-FILM GROWTH BY INTERNAL-STRESS MEASUREMENT UNDER ULTRAHIGH-VACUUM CONDITIONS - SILVER AND COPPER UNDER THE INFLUENCE OF OXYGEN*. Thin Solid Films, 1986. **142**(1): p. 65-76.
15. Chen, K.S. and K.S. Ou, *Modification of curvature-based thin-film residual stress measurement for MEMS applications*. Journal of Micromechanics and Microengineering, 2002. **12**(6): p. 917-924.
16. Ma, C.H., J.H. Huang, and H. Chen, *Residual stress measurement in textured thin film by grazing-incidence X-ray diffraction*. Thin Solid Films, 2002. **418**(2): p. 73-78.
17. Di, Y.X., et al., *Residual stress measurement of porous silicon thin film by substrate curvature method*. Acta Physica Sinica, 2006. **55**(10): p. 5451-5454.
18. Chowdhury, S. and M.T. Laugier, *Thin film stress measurement by instrumented optical fibre displacement sensor*. Applied Surface Science, 2007. **253**(9): p. 4289-4294.
19. Malhotra, S.G., et al., *Analysis of thin film stress measurement techniques*. Thin Solid Films, 1997. **301**(1-2): p. 45-54.
20. Malhotra, S.G., et al., *Depth dependence of residual strains in polycrystalline Mo thin films using high-resolution x-ray diffraction*. Journal of Applied Physics, 1996. **79**(9): p. 6872-6879.
21. Flinn, P.A., D.S. Gardner, and W.D. Nix, *MEASUREMENT AND INTERPRETATION OF STRESS IN ALUMINUM-BASED METALLIZATION AS A FUNCTION OF THERMAL HISTORY*. Ieee Transactions on Electron Devices, 1987. **34**(3): p. 689-699.
22. Sutmann, G., *Classical Molecular Dynamics*. NIC Series, 2002. **10**: p. 211-254.
23. Allen, M.P., *Introduction to Molecular Dynamics Simulation*. NIC Series, 2004. **23**: p. 1-28.
24. Del Vecchio, A.L. and F. Spaepen, *The effect of deposition rate on the intrinsic stress in copper and silver thin films*. Journal of Applied Physics, 2007. **101**(6): p. 063518.

25. Zhang, D., et al., *Influence of kinetic energy and substrate temperature on thin film growth in pulsed laser deposition*. Surface and Coatings Technology, 2006. **200**(12-13): p. 4027-4031.

VITA

Name: Haifeng Zheng

Date of Birth: June 3rd, 1986

Place of Birth: Guangdong, China

Parents: Wei Zheng and Juan Chen

Education:

M.S. Mechanical Engineering and Mechanics, Lehigh University, PA, USA, September 2011

Thesis: “Molecular Dynamic Simulation of Thin Film Growth Stress Evolution”

B.S. Safety Engineering, South China University of Technology, China, June 2005

Publications:

An Incorporated Design of the Fin-and-Tube Heat Exchanger (China patent #: CN201322562)